

Flash Infrared Thermography Contrast Data Analysis Technique

Engineering Directorate
Structural Engineering Division
Materials and Processes Branch

December 2009



National Aeronautics and
Space Administration

Lyndon B. Johnson Space Center
Houston, Texas 77058

Flash Infrared Thermography Contrast Data Analysis Technique

Prepared by:

Ajay Koshti

12/02/2009

Ajay M. Koshti, ES4
Materials and Processes
Branch/ES4

Date

Reviewed by:

Chelakara Subramanian

12/02/2009

Chelakara Subramanian, Ph. D.,
P. Eng (UK), FIEE
Professor, Florida Institute of
Technology Melbourne, FL

Date

Approved by:

Bradley S. Files

12/3/09

Bradley S. Files
Chief, Materials and Processes
Branch/ES4

Date

TABLE OF CONTENTS

Abstract.....	1
1. Introduction.....	1
2. Flash Thermography Equipment.....	2
3. One-Sided Flash Thermography Technique	2
4. IR Flash Thermography Anomaly Detection	3
5. Flash Thermography IR Data Analysis Using Commercial Software	4
6. IR Contrast Objectives	5
7. Normalized Contrast Definition.....	6
8. Contrast Extraction	8
9. Contrast Imaging.....	9
10. IR Contrast Thermal Measurements and Related Terminology.....	11
11. Contrast Simulation	13
12. Half-max Width Estimation.....	18
13. Amplitude Ratio.....	19
14. Calibration Steps in the IR Contrast Application	20
15. Calibration Curves for RCC.....	20
16. Calibration for Specified Attenuation ($\% \mu$) for a Thin Delamination	23
17. Calibration Curves for Contrast Attenuation	25
18. Contrast Maps for the Attenuated Calibrations	27
19. Similarities and Differences between Flash Thermography IR Contrast Analysis and Ultrasonic Pulse Echo Analysis	30
20. Case Study: RCC Joggle Area Test Pieces with Subsurface Delaminations	32
21. Conclusions.....	46
22. Recommendation for Analyzing Linear Delaminations.....	46
ACKNOWLEDGEMENTS	48
APPENDIX: Calibration Steps in the IR Contrast Application.....	50

LIST OF FIGURES

Figure 1: Schematic of Flash Thermography Set-up	2
Figure 2: Measurement and Reference Regions of Interest (ROI)	3
Figure 3: IR Image Showing Indications of Flat-Bottom Holes in Standard 03-48	7
Figure 4: Example of Data File for Single Pair of Measurement and Reference Point	7
Figure 5: Unprocessed Datacube	10
Figure 6: IR Contrast Processed Datacube	10
Figure 7: Example of Raw Contrast Evolution from a Flat Bottom Hole	11
Figure 8: Flaw Size Parameter A_c	14
Figure 9: Example of Correlation of Calibration Constants to Flaw Size Parameter	15
Figure 10: Example of Filtered Contrast Evolution from a Flat Bottom Hole	15
Figure 11: Example of Predicted Contrast Evolution from a Flat Bottom Hole	16
Figure 12: Three Contrast Evolutions (Raw, Filtered and Prediction) Overlaid for Comparison	17
Figure 13: Main Interface for IR Contrast Application with the Three Evolutions and the Calibration Set-up Window	17
Figure 14: Half-max Width Measurement Technique Width Ratio	18
Figure 15: Images of Calibration Standard D2	20
Figure 16: Calibration Curve from Base Depth Holes	21
Figure 17: Depth Constant versus the Depth Ratio	21
Figure 18: Amplitude Factor versus the Depth Ratio	22
Figure 19: Results of Depth Calibration on RCC Standard D1 (0.025 in deep holes) and D2 (0.050 in deep holes)	22
Figure 20: Results of Diameter Calibration on RCC Standard D1 (0.025 in deep holes) and D2 (0.050 in deep holes)	23
Figure 21: An Example of Relationship between Peak Time Ratio and Peak Contrast Ratio Based on ThermoCalc Simulation for void depth of 0.040 in.	24
Figure 22: An Example of Calibration Curves for No Attenuation, 30 Percent Attenuation and 50 Percent Attenuation	26
Figure 23: Seventy Percent Attenuation Calibration Curves Estimated by Extrapolating Calibration Curves from Fig. 22	26
Figure 24: Peak Contrast versus Peak Time Contrast Map for 0 Percent Attenuation (EFBH)	27
Figure 25: Peak Contrast versus Peak Time Map for 50 Percent Attenuation (EUG)	28
Figure 26: Slot Specimen, IR Image at 0.67 sec of Hole 3 (Top), Hole 4 (Middle) and Hole 5 (Bottom) and Their Half-Max Vertical Boundary	29
Figure 27: Comparison of Actual Width with Predicted EFBH Diameters for Holes 3, 4 and 5 (File: Right threeslots.xls)	29
Figure 28: IR Image of RCC Joggle Area Anomaly	32
Figure 29: Contrast Extraction Locations and Half-max Boundary	33
Figure 30: Typical Contrast Evolution without Craze Crack Influence	34
Figure 31: Typical Contrast Evolution with Craze Crack Influence	34
Figure 32: Typical Contrast Evolution with Craze Crack Influence, Second Peak Less Distinct	35

Figure 33: Contrast Evolution with Craze Crack Influence, No Second Peak	35
Figure 34: Peak Contrast along the Indication	36
Figure 35: Peak Time along the Indication	36
Figure 36: Persistence Energy Time along the Indication	37
Figure 37: EFBH Diameter, Depth and Half-max Width Estimations	37
Figure 38: IR Contrast Diameter and Depth Prediction	38
Figure 39: Comparison of EFBH Diameter and Adjusted 50 Percent Attenuation EUG Diameter	39
Figure 40: Inverse of Gamma Square Variation along the Y-Location	39
Figure 41: Example of Use of Peak Product Time as a Parameter Related to EFBH/EUG Diameter	40
Figure 42: Example of Use of Peak Time to Contrast Ratio as a Parameter Related to EFBH/EUG Depth	40
Figure 43: Typical Schematic of Cross Section of the Specimen	41
Figure 44: Experimental Data of Measured Gap Thickness versus the Width Ratio on Linear Indications	44
Figure 45: Peak Product Time/Width ^{2.3} versus Gap Thickness on Square Voids Using ThermoCalc Simulation	45
Figure. 46: Experimental Data of Peak Product Time/Half-max Width ² versus Measured Gap Thickness on Linear Voids in RCC	45

Flash Infrared Thermography Contrast Data Analysis Technique

Abstract

This paper provides information on an IR Contrast technique that involves extracting normalized contrast versus time evolutions from the flash thermography inspection infrared video data. The analysis calculates thermal measurement features from the contrast evolution. In addition, simulation of the contrast evolution is achieved through calibration on measured contrast evolutions from many flat-bottom holes in the subject material. The measurement features and the contrast simulation are used to evaluate flash thermography data in order to characterize delamination-like anomalies. The thermal measurement features relate to the anomaly characteristics. The contrast evolution simulation is matched to the measured contrast evolution over an anomaly to provide an assessment of the anomaly depth and width which correspond to the depth and diameter of the equivalent flat-bottom hole (EFBH) similar to that used as input to the simulation. A similar analysis, in terms of diameter and depth of an equivalent uniform gap (EUG) providing a best match with the measured contrast evolution, is also provided. An edge detection technique called the half-max is used to measure width and length of the anomaly. Results of the half-max width and the EFBH/EUG diameter are compared to evaluate the anomaly. The information provided here is geared towards explaining the IR Contrast technique. Results from a limited amount of validation data on reinforced carbon-carbon (RCC) hardware are included in this paper.

1. Introduction

Infrared (IR) Flash thermography is a Nondestructive Evaluation (NDE) method used in the inspection of thin nonmetallic materials such as laminated composites in the aerospace industry. It is primarily used to detect delamination-like anomalies, although surface cracks are also detectable to some extent. In most circumstances, a single-sided or reflection technique is used where the flash lamp (heat source) and the IR camera (detector) are on the same side of the part (test object) inspected. In some situations, a through-transmission or two-sided flash thermography technique is used. In the through-transmission technique, the source and the detector are on the opposite sides of the part. The area of the part under inspection has constant part thickness in the through-transmission flash thermography. Maldague¹ provides general information on flash thermography including practical examples and mathematical analysis. Carslaw and Jaeger² provide analytical solutions for thermal conduction in an isotropic material for many cases of heat sources and boundary conditions. Spicer³ provides information on both theory and applications in active thermography for nondestructive evaluation. This paper deals only with the single-sided flash thermography.

2. Flash Thermography Equipment

The IR Flash thermography equipment consists of a flash-hood, flash power supply/trigger unit, flash duration controller, camera data acquisition electronics and a personal computer (PC). The PC is used for controlling the flash trigger, camera data acquisition, data display and post processing of the acquired data. The flash-hood is made from sheet metal. One of the six sides of the hood is open. The side opposite to the open side has a hole in the center to provide a window for the lens of the IR camera which is mounted from outside of the hood. The IR camera is focused at the test object (part) surface located at the hood opening. Two flash lamps are located at the inner wall of the hood on the camera side. These flash lamps direct the illumination towards the hood opening where the part is located without directly shining the light into the camera lens. The hood contains most of the intense flash. See Fig. 1.

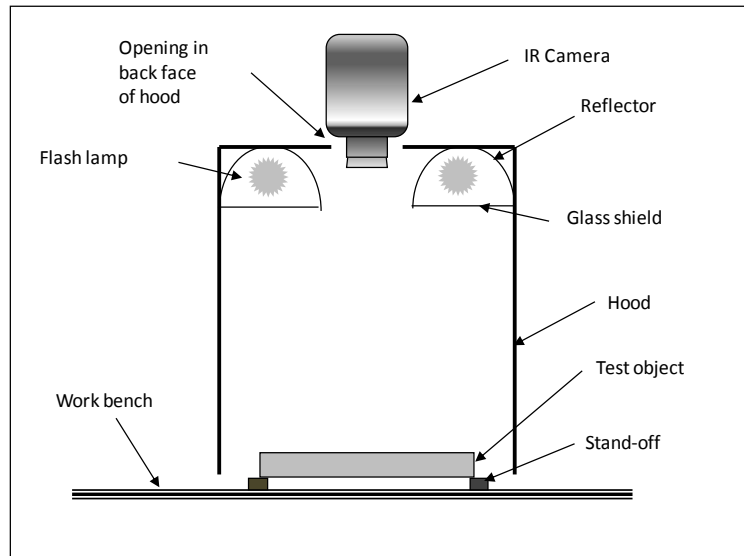


Figure 1: Schematic of Flash Thermography Set-up

3. One-Sided Flash Thermography Technique

If the test object can be accommodated inside the hood, then it is located at the hood opening or slightly inside the hood. Otherwise, the part is located slightly outside of the hood opening. A short duration (e.g. 5 msec), intense (12 kJ) flash is triggered using the computer keyboard. The data acquisition is triggered a few seconds before the flash and it continues until the prescribed time. The camera provides a sequence of IR images (or frames) called the datacube of the part surface taken at the chosen frame rate (e.g. 60 Hz or 60 frames per sec). The intensity (numerical value) of each pixel in the image is a function of the surface temperature of the corresponding area on the part at the time of the image frame. The flash causes the surface to warm up slightly and the heat starts to

dissipate rapidly. The surface cools through thermal radiation, convection and conduction. It is assumed that the heat conduction within the part is the dominant heat transfer mode until the temperature gradients within the part become small. At later times, the heat conduction is of the order of the combined effect of heat convection and radiation. The IR data acquisition and data analysis utilizes the thermal data in the short duration immediately after the flash where the thermal dissipation is dominated by the heat conduction (adiabatic process) within the part. Metallic and thin non-metallic specimens can be often considered as adiabatic, i.e. the convection heat exchange coefficient value can be assumed zero in these cases. The limit in specimen properties for considering the adiabatic case is given with the following expression that is well-known in the heat conduction theory:

$$Bi = \frac{hL}{K} \leq 0.1.$$

Here, L is the specimen thickness, K is the specimen conductivity and Bi is the Biot number.

4. IR Flash Thermography Anomaly Detection

Let us assume that the part is a plate made of a thermally isotropic material with constant thickness and it fits inside the hood. The plate is supported at the corners on insulating standoffs and the hood is oriented vertically. If we assume that the flash intensity is uniform over the plate top surface, then the heat conduction will be in a direction normal to the part surface in most of the acreage area (area away from edges of the part and flash boundary). The heat is conducted uniformly from the top surface to the bottom surface of the plate. The normal heat conduction will be obstructed by an anomaly such as a small round gapping delamination at the center of a plate, as depicted in Fig. 2. The volume bounded by the anomaly on one side and the part top surface on the other side is called the heat trapping volume.

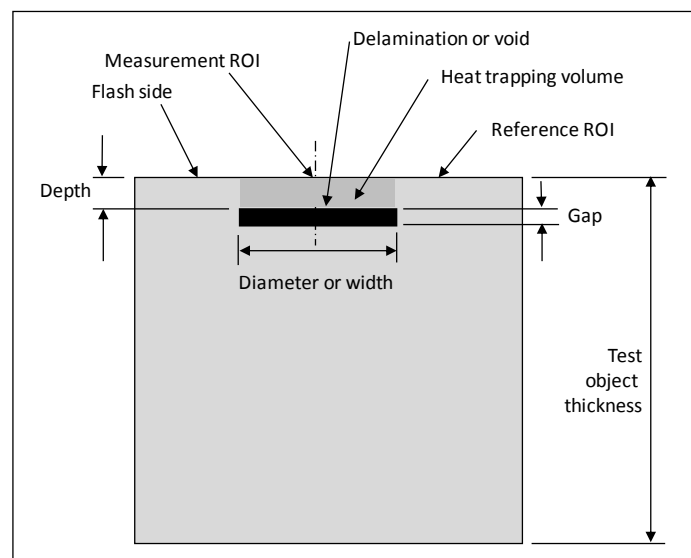


Figure 2: Measurement and Reference Regions of Interest (ROI)

The top surface area surrounding the anomaly cools faster than the top surface (footprint) area above the anomaly. The IR camera captures the surface temperature image in terms of the pixel intensity and shows the anomaly as a hot spot (e.g. an area warmer than the surrounding area) which is about the size and shape of the anomaly footprint. Relative pixel intensity of the hot spot changes with the time. Deeper anomalies appear at later times in the IR video compared to the near surface anomalies. After the appearance of an anomaly in the IR video, its relative pixel intensity continues to increase with time. The relative pixel intensity of the anomaly reaches a peak at a certain time and then the relative intensity decays until the indication area temperature and the surrounding area temperature become equal. Figure 3 shows an IR image of a plate with round flat-bottom holes (FBH's) machined from the back side to simulate gapping delaminations of differing depths. The part continues to cool down to ambient temperature through heat convection and radiation. If any objects contact the part or the part has significant area that does not receive the flash, then the heat conduction to unflashed area or to the contacting object also causes cooling.

5. Flash Thermography IR Data Analysis Using Commercial Software

Commercially available IR data analysis software analyzes the data to detect the anomalies by providing enhanced processed images. Commercial software EchoTherm⁴ and Mosaic⁴ by Thermal Wave Imaging Inc., provide many post-processing options such as, frame subtraction from other frames, frame averaging, pixel intensity rescaling etc. They also provide first and second derivative images of the pixel intensity with respect to the frame number or time. The derivative images are drawn from fitted data. The fitted data is created by fitting curves in the pixel intensity versus time profile of each pixel. The pixel intensity (average of one or more neighboring pixels) versus time ($T-t$) curve can be displayed in logarithmic (log-log) scale. An ideal temperature-time decay log-log curve¹ on a thick plate with no anomalies is a straight line with a slope of -0.5. The measured log-log curve on an anomaly would have a constant negative slope for some time after the flash but at a time related to the heat transit time to the anomaly, the decay curve would depart from the linear constant slope (see ASTM E 2582). The departure time or the early appearance time (t_{appear}) can be used to estimate the depth of the anomaly. The software also allows a calibration of a ruler for measuring the distance between the pixels and provides the pixel coordinates. Thermofit Pro⁵ also provides many of the above image post-processing routines such as derivatives of pixel intensities. This software also defines a running contrast and normalized contrast. The definition of Thermofit Pro normalized contrast is different than used in this paper. The Thermofit Pro software does not define normalized image contrast and the normalized temperature contrast separately and therefore does not make distinction between the two. Both EchoTherm and Thermofit Pro implicitly assume that the pixel intensity is proportional to the surface temperature and is a complete indicator of the surface temperature.

The EchoTherm software provides simple pixel “contrast”, which is defined as the difference in the pixel intensity of any two selected areas on the test object surface. The

ThermoCalc simulation provides simple temperature “contrast” which is defined as the difference in the temperature of any two selected areas on the test object surface. The simple contrast evolution looks similar to the normalized contrast, but is not as useful to correlate to the flaw parameters due to its dependence on flash intensity.

6. IR Contrast Objectives

The subject simulation model, software application, data analysis technique and approach are named “IR Contrast” by the author. The IR Contrast technique is geared towards anomaly characterization and not towards detection. The IR Contrast approach relates thermal measurements, such as the contrast evolution (or contrast signal) amplitude of an anomaly, in terms of the normalized anomaly contrast as a function of the frame number or the post-flash time. Under some constraints, the normalized anomaly contrast is mainly influenced by factors related to an anomaly such as the material thermal properties (diffusivity and emissivity), anomaly size, depth and gap thickness (heat transmissivity or thermal mismatch factor). The contrast is also affected by factors that are unrelated to the anomaly such as the part curvature, uneven part cross section, changing thermal properties along the part surface, surface cracks, surface texture, uneven flash heating, camera pixel size, focusing and proximity to the part edge or the flash boundary. The contrast signal amplitude is proportional to temperature rise above the ambient temperature. Therefore, the ambient temperature is not considered to be a significant factor. Also, we assume a natural heat convection which has a very small and constant effect on the contrast evolution. The net effect of the unrelated factors on the contrast evolution is assumed to be small and constant. The IR Contrast technique seeks to either minimize the effect of the unrelated factors in order to improve accuracy of the IR Contrast analysis or to control the unrelated factors to improve repeatability of the IR Contrast analysis. The experimental evolutions are used in the calibration of the predicted contrast evolution and account for the effect of the unrelated factors to some extent. Several amplitude and time-related thermal measurements (e.g. peak contrast and peak contrast time, peak product time, persistence energy time etc.) are computed from the measured contrast evolution. These parameters bear some correlation to the anomaly depth, width and gap (or heat transmissivity through the anomaly). The approach also involves measurement of width of the indication using the half-max technique explained later.

The IR Contrast also uses calibrated simulation of the contrast evolution. The software iteratively calculates the diameter and depth as input, called equivalent flat-bottom hole (EFBH) inputs, to the simulation that provides the best match to the measured contrast evolution. Thus, the anomaly depth and width are mapped into an EFBH diameter and depth. It is hypothesized that if the ratio of EFBH diameter to half-max diameter on a round anomaly is close to one, then the anomaly is similar to a FBH or a gapping round delamination. Similarly, if the ratio of EUG diameter to half-max diameter on a round anomaly is close to one, then the anomaly is similar to a round void with uniform gap. It

is hypothesized that the EFBH depth is an estimation of the anomaly depth if the anomaly is similar to a gapping delamination or a FBH. Similarly, the EUG depth is an estimation of the anomaly depth if the anomaly is similar to a void with a uniform gap. The IR Contrast allows better characterization of the anomaly in terms of anomaly depth and width and the gap thickness. The IR Contrast application is programmed for many materials and therefore provides a quick approximate prediction of the contrast on a given delamination-like anomaly. It can be used as a training tool for the application of flash thermography.

7. Normalized Contrast Definition

The normalized contrast is defined as,

$$\bar{C}^t \equiv \frac{(T - T^0) - (T_R - T_R^0)}{(T - T^0) + (T_R - T_R^0)}, \quad (1)$$

where, \bar{C}^t = normalized contrast or modulation contrast. It is a function of the post flash time, t . The time is measured from the moment of the flash (e.g. flash time = 0).

T = IR camera pixel intensity at the measurement point (region of interest (ROI)) of the anomaly

T_R = pixel intensity at the anomaly reference point or ROI,

T^0 = pixel intensity in the measurement ROI of the anomaly before flash,

T_R^0 = pixel intensity of the reference ROI before flash.

Any selected region (point or area) where pixel intensity is measured is referred to as the region of interest (ROI)

Figures 3 and 4 depict the location of the measurement and reference ROI's and an example of a contrast data file.

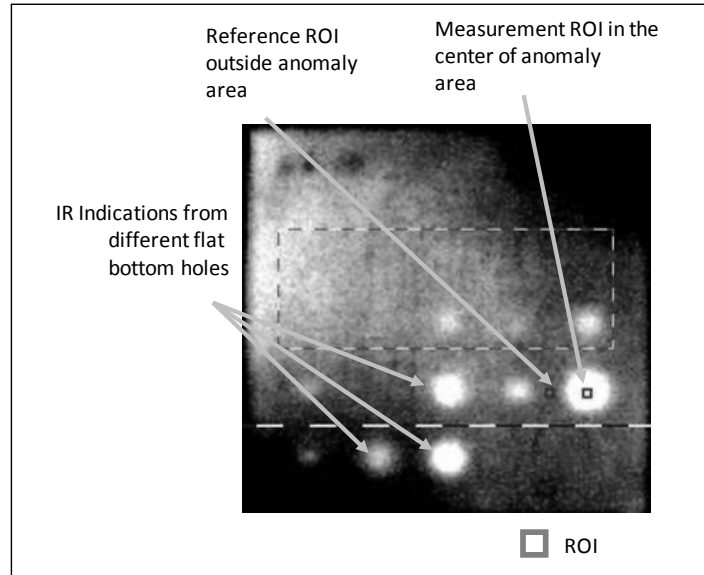


Figure 3: IR Image Showing Indications of Flat-Bottom Holes in Standard 03-48

Eq. 1 can be written as,

$$\bar{C}^t = \frac{\Delta T - \Delta T_R}{\Delta T + \Delta T_R}, \tag{2}$$

where, $\Delta T = T - T^0 =$ pixel intensity rise at the measurement ROI of the anomaly at time t ,

$\Delta T_R = T_R - T_R^0 =$ pixel intensity rise at the reference ROI at time t .

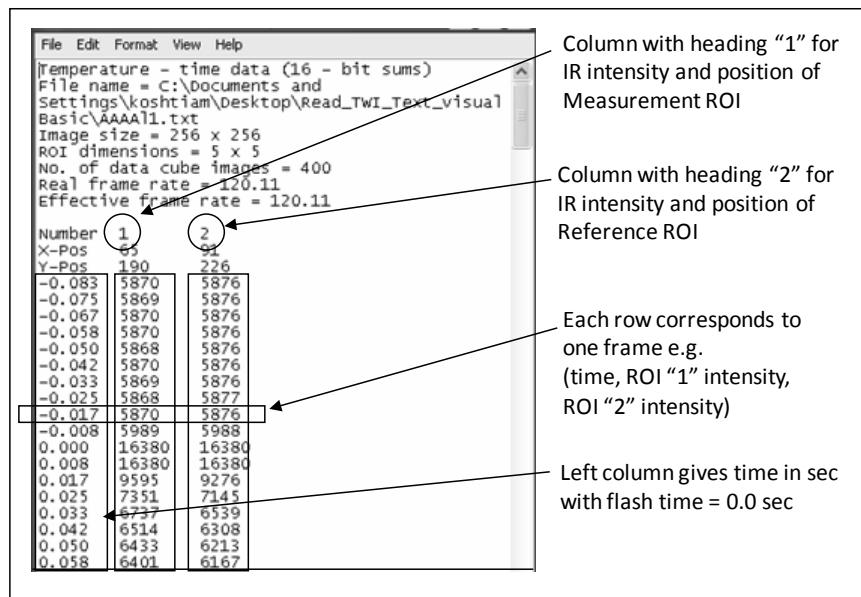


Figure 4: Example of Data File for Single Pair of Measurement and Reference Point

Thus, the normalized IR Contrast is defined as the ratio of the difference in pixel intensity rise between the anomaly measurement point and the reference point and the sum of the two pixel intensity rises. This definition is similar to the definition of signal modulation and the values would range from -1 to +1 in normal situations. In some abnormal situations the values beyond customary range of -1 to +1 are possible and are outside the domain of this analysis. In normal measurement situations, the reference area is always cooler than the anomaly area. Therefore, the contrast shall always be positive. But in practice, a surface heat gradient caused by factors including the proximity of the anomaly to the edge of the flash zone or uneven thickness of the cross section may cause the anomaly to appear cooler at later times compared to temperature of the reference area. Limits on the proximity of region of interest to a physical boundary, illumination boundary and part curvature can be determined by investigating the surface pixel intensity profiles and the contrast evolutions. The pre-flash surface temperature distribution and emissivity variation also affect the contrast.

Ideally, $T^0 = T_R^0$ and Eq. 2 simplifies to,

$$\bar{C}^t = \frac{T - T_R}{T + T_R - 2T^0}. \quad (3)$$

The subtraction of pre-flash pixel intensity and the division by the denominator in the contrast definition normalizes the numerator. The contrast increases rapidly after the flash reaching its peak value and then slowly diminishes and achieves a constant level. In practice, the contrast should ultimately reach a zero value when the temperature equalizes in the part if we assume a constant and high emissivity (>0.85) and the same pre-flash temperature in the area of contrast measurement. For low emissivity parts like metals a high emissivity paint or coating can be applied temporarily to the surface and then the flash thermography data acquisition can be undertaken.

8. Contrast Extraction

Extraction of the contrast evolution involves choosing the measurement and the reference points in the datacube. The measurement point is chosen to be the highest intensity pixel. Usually, the frame chosen for this detection is close to t_{peak} (defined later). For round indications, the measurement point is mostly located closed to the center (or centroid) of the anomaly footprint. For elongated anomalies, several measurement points located close to the longitudinal centerline of the indication are chosen. This technique yields repeatable locations of measurement points. Selection of the reference point has many possibilities in terms of relative location (radial distance and angular orientation) with respect to the measurement point. Selection of the optimum reference point or points involves choice of reference points that provides a contrast evolution that is closest to the ideal contrast evolution. The ideal contrast evolution is defined as the evolution with maximum possible amplitude from the same anomaly if the anomaly were located in the

areage area in an ideal material (flat surface, uniform emissivity and diffusivity) under ideal flash exposure and IR data acquisition conditions as were used during the calibration. Here, the IR setup seeks uniformity in the pre-flash temperature, even flash distribution and minimization of the lateral temperature gradients not related to the anomaly.

One of the techniques involves searching for the reference points that provides leveling of the contrast evolution. A leveled contrast evolution has the contrast value equal to zero at later times (t_{tail} defined later). It is desirable to extract a level contrast evolution within constraints on the relative location and size of the reference point. Combining (e.g. averaging) of more than one reference point to provide a composite reference point can be beneficial in leveling the extracted contrast evolution. The IR Contrast application allows post-extraction (artificial) leveling correction by shifting the contrast evolution up or down. The post-extraction contrast leveling should be used cautiously with the support of the validation data. The post-extraction contrast leveling is not likely to be as effective as the contrast leveling during (or prior to) the contrast extraction. If extraction of the level contrast evolution is not practical, then other schemes such as fixing the relative distance/orientation of the reference point can be employed. The scheme provides a repeatable non-leveled contrast evolution which may be leveled artificially. Here, the contrast evolution may not provide the most accurate measurements or prediction but is likely to yield repeatable measurements that differ consistently from ideal contrast measurements. If the variability of the difference is assessed statistically in a given application, then it may be possible to apply corrections to the contrast measurements and estimations.

9. Contrast Imaging

A separate contrast imaging application was written to work with EchoTherm. The application allows choice of the reference area and then converts the raw datacube into the contrast datacube using the reference area. The pixel intensity versus time evolution of each pixel is replaced by the normalized contrast versus time evolution. The contrast datacube images look similar to raw datacube images. Figure 5 shows a frame from a raw datacube with pixel intensity versus time curves at selected regions of interest (ROI's). Here, all pixels are used as the measurement pixels. Thus, the pixels within the reference ROI would have a contrast value of zero or close to zero.

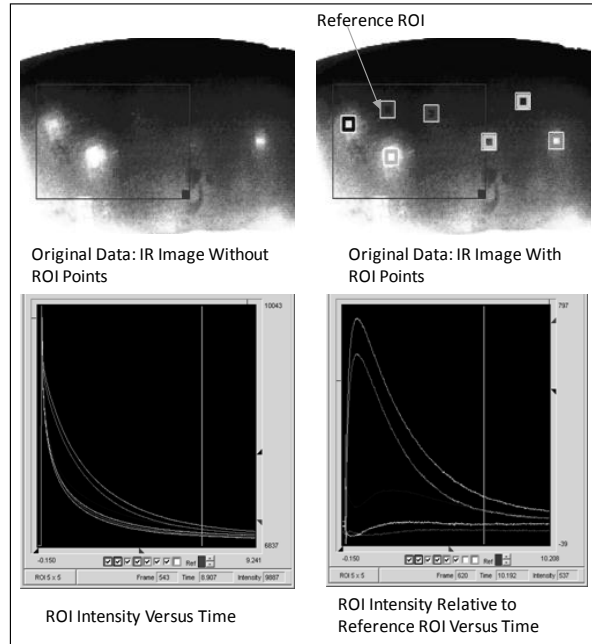


Figure 5: Unprocessed Datacube

The chosen reference ROI is shown in Fig. 5. Figure 6 shows a frame from the contrast datacube with the contrast versus time curves at the selected ROI's. The contrast datacube allows a quick view of the contrast evolution and forms the basis for the feature images based on signal processing (e.g. filtering) and the thermal measurements (e.g. peak time) defined below.

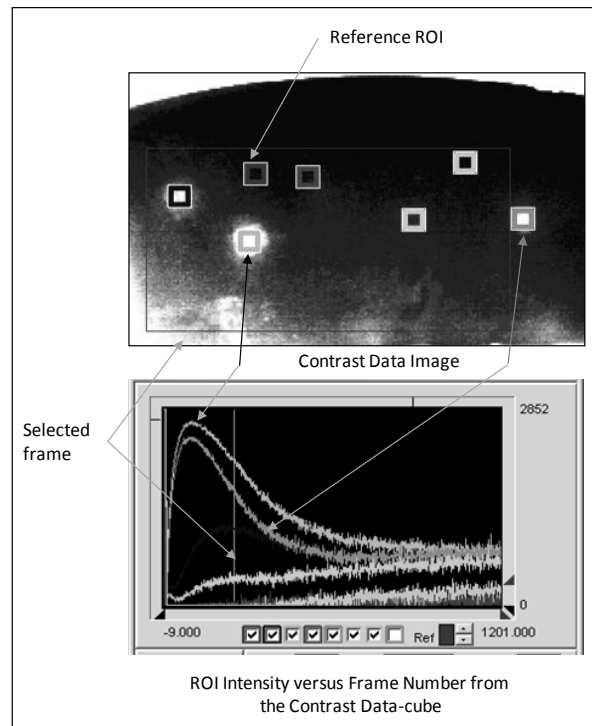


Figure 6: IR Contrast Processed Datacube

10. IR Contrast Thermal Measurements and Related Terminology

Apart from using the simulation contrast, the IR Contrast technique involves thermal feature measurements on the IR Contrast evolution. Explanation of each measurement terminology follows.

Peak Contrast, \bar{C}_a^{peak} : Peak contrast is defined as the amplitude or value of the highest point in the contrast evolution. It may also be referred to as amplitude or peak amplitude. See Fig. 7.

Peak Contrast Time (sec), t_{peak} : Peak contrast time is defined as the time at which the peak of the contrast evolution occurs. The time measurement starts from the flash time. See Fig. 7.

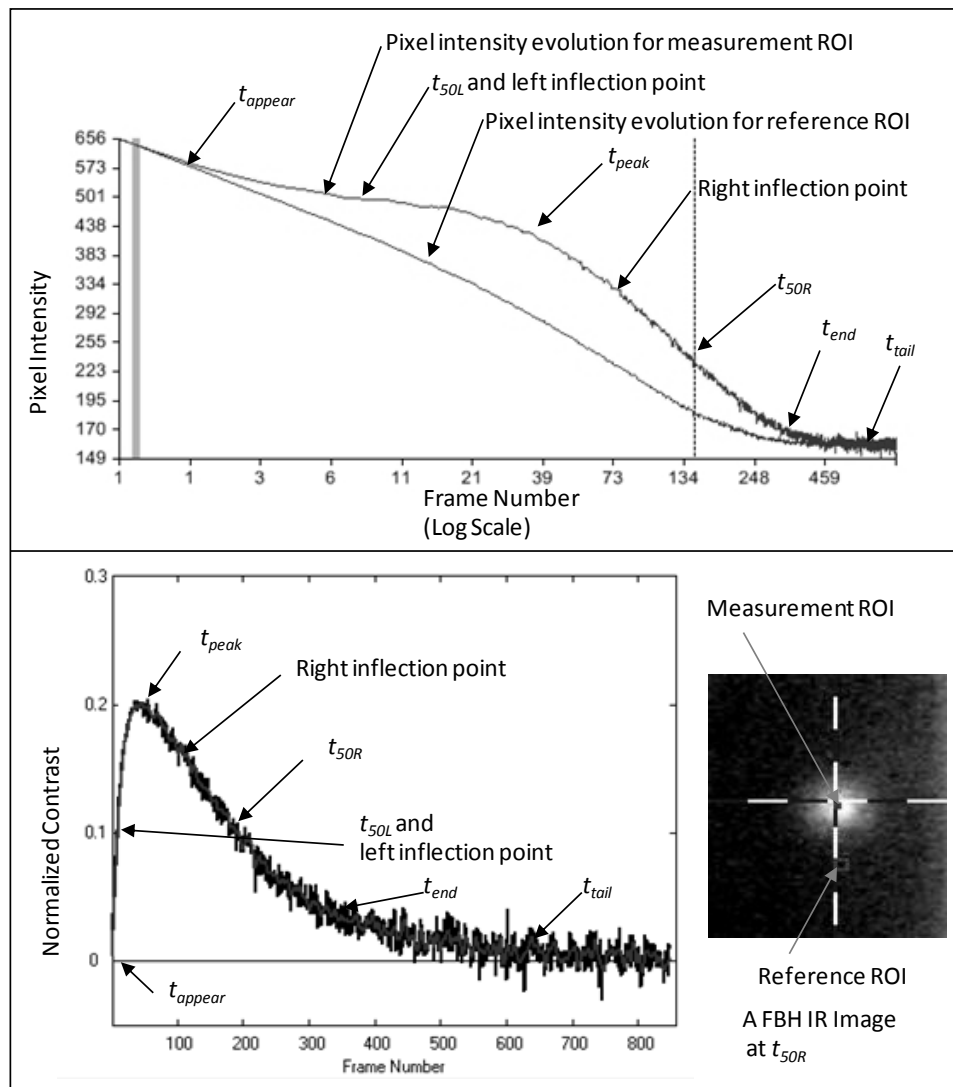


Figure 7: Example of Raw Contrast Evolution from a Flat Bottom Hole

Fifty Percent Left of Peak Time (Sec), t_{50L} : This is the time at which the 50 percent of peak contrast occurs before the peak contrast time.

Fifty Percent Right of Peak Time, t_{50R} : This is the time at which the 50 percent of peak contrast occurs after the peak contrast time.

Ten Percent Right of Peak Time, t_{10R} : This is the time at which the 10 percent of peak contrast occurs after the peak contrast time.

End Time, t_{end} : This is the time used to determine the right limit point in the time range for comparison of the measured contrast with the simulation contrast.

$$t_{end} = 2t_{50R} - t_{peak} \quad (4)$$

Tail Time, t_{tail} : Another time used in leveling of the contrast signals or in optimizing the location of the reference points. The IR Contrast model assumes that the contrast value is nearly zero at the t_{tail} time.

$$t_{tail} = 3t_{50R} - 2t_{peak} \quad (5)$$

Fifty Percent Persistence Time, $t_{50L-50R}$: This is the time between t_{50L} and t_{50R} ,

$$t_{50L-50R} = t_{50R} - t_{50L} \quad (6)$$

The times defining the persistence can be different (e.g. $t_{50L-10R}$).

Withholding Heat Time, $t_{wh,50L-50R}$ (sec):

$$t_{wh,50L-50R} = \bar{C}_a^{peak} t_{50L-50R} \quad (7a)$$

Withholding heat time is a measure of area under the contrast curve.

Persistence Energy Time, $t_{E,50L-50R}$ (sec):

$$t_{E,50L-50R} = \frac{\sum_{n_{50L}}^{n_{50R}} \bar{C}_a}{\nu} \quad (7b)$$

where, ν = the frame rate in frames/sec (Hz). n_{50L} and n_{50R} are the frame numbers corresponding to times t_{50L} and t_{50R} respectively. These frame numbers could be different as chosen by the user (e.g. n_{50L} to n_{10R} ; n_{50L} to n_{peak} ; or n_1 to n_2). Depending upon the choice of the starting frame number and ending frame number in relation to the peak time, the integrated times of Eq. (7b) may be denoted as the rise energy time, decay energy time, etc. In many inspection situations, especially for thin parts, use of the rise energy time may be appropriate as the rise time is much shorter than the decay times.

Also, if the anomaly depth is expected to be constant, integrating between fixed frames (e.g. n1 and n2) is useful especially within the rise time window. Both the persistence energy time and the withholding heat time are related to the heat trapping volume or the depth and diameter of the anomaly.

Two other important quantities based on the time are defined. These are the peak product time and the peak time to contrast ratio (or peak time per unit peak contrast). The peak product time is given by,

$$t_{product} = \bar{C}_a^{peak} t_{peak}. \quad (8a)$$

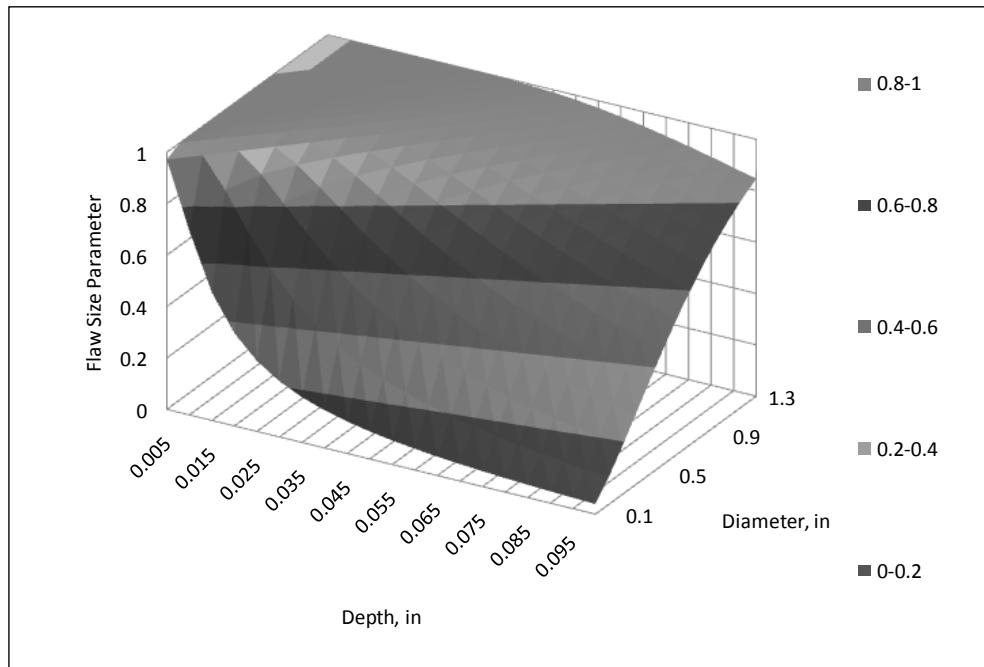
The peak time to contrast ratio is given by,

$$t_{t,C} = \frac{t_{peak}}{\bar{C}_a^{peak}}. \quad (8b)$$

From contrast maps (Figs. 24 and 25), it is evident that the peak product time is related to the diameter of EFBH (or EUG) and peak time to contrast ratio is related to depth of the EFBH (or EUG). Thus, these measurements are very useful if simulation analysis is not performed. A smoothed contrast evolution and even simulation fit can provide more stable detection of the peak point in the contrast evolution compared to the peak detection on the raw contrast evolution. Therefore, for more repeatable and reliable measurements, a smoothed evolution or the simulation fit evolution is recommended. In many situations, the raw evolution may not have a peak corresponding to the subsurface anomaly due to influence of the texture. In such a situation, use of a simulation fit evolution that is fitted to the subsurface portion of the raw contrast evolution may be better due to higher confidence in locating the peak and computing the quantities in Eqs. (8a) and (8b).

11. Contrast Simulation

The contrast simulation uses a quantity called the flaw size parameter, A_c , which is a function of the anomaly depth and diameter. It is a measure of anomaly size and is shown in Fig. 8. The peak product time, persistence energy time, withholding heat time and the peak contrast are measures of the contrast signal strength. Therefore, these measurements are candidates for conventional probability of detection (POD) analysis where correlation between the signal response and the flaw size is analyzed. Although the flaw size parameter A_c is internal to the IR Contrast model, its value is displayed as it plays an important role in demonstrating correlation between the anomaly size and the IR Contrast thermal measurements as well as the EFBH predictions. The flaw size parameter can be used as the flaw size for the POD analysis.

Figure 8: Flaw Size Parameter A_c

The IR Contrast simulation assumes that the flaws are located at a shallow depth compared to the part thickness. It also assumes that the part thickness is considered to be very thick (\gg threshold thickness⁷). Calibration parameters such as the depth constant, diameter constant, amplitude constant and the amplitude factor are used in the simulation application. The depth constant is used to calibrate for the thermal diffusivity. The diameter and amplitude constants are functions of the flaw size parameter. The relationships between the flaw size parameter and the two constants are called the calibration curves. The calibration curves for the two constants are established by matching the simulation to the measured contrast of many FBH's in the material of interest. These calibration constants are dimensionless. See Fig. 9 for sample calibration curves.

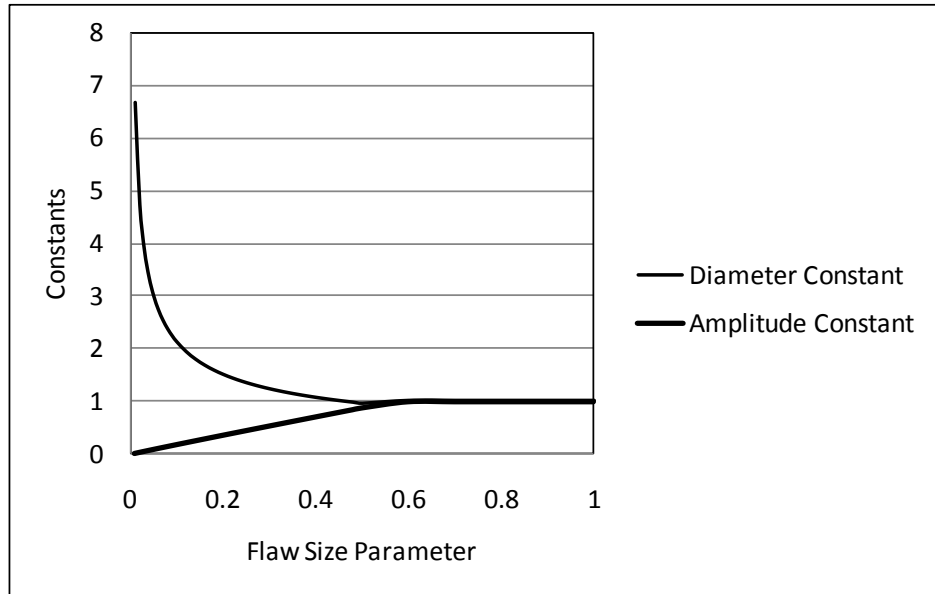


Figure 9: Example of Correlation of Calibration Constants to Flaw Size Parameter

The product of the peak time and persistence time provides a correlation to the product of depth and diameter. The withholding heat time and persistence energy time capture the strength of the IR indication to draw attention for further analysis. Shallow anomalies have shorter persistence but higher amplitude. Deeper anomalies have lower amplitude. Wider anomalies have longer persistence. The persistence energy time includes part of the evolution containing the peak amplitude.

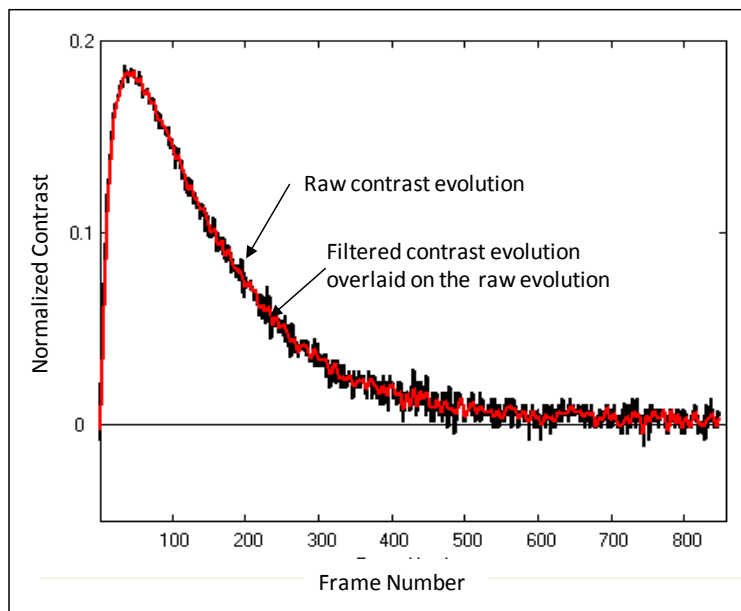


Figure 10: Example of Filtered Contrast Evolution from a Flat Bottom Hole

The raw contrast data contains the camera noise. The signal can be filtered by a signal processing routine to improve the IR Contrast calculations. The filtered contrast is shown

in gray and the raw contrast is shown in black in Fig. 10. See also Fig. 13 which is in color. Figure 11 shows the predicted contrast curve that provides the best match to the measured contrast evolution. The EFBH depth and diameter input to the simulation providing the best match to measured contrast data is obtained in an automated way. The IR Contrast application calculates the approximate depth and diameter of the EFBH directly based on the peak contrast, peak contrast time and other times including t_{50L} , t_{50R} and t_{10R} . The simulation matching provides an indirect method of assessing the EFBH depth and diameter. Figure 12 shows the raw contrast, filtered contrast and the simulation contrast evolutions plotted on the same graph. See also Fig. 13 which is in color.

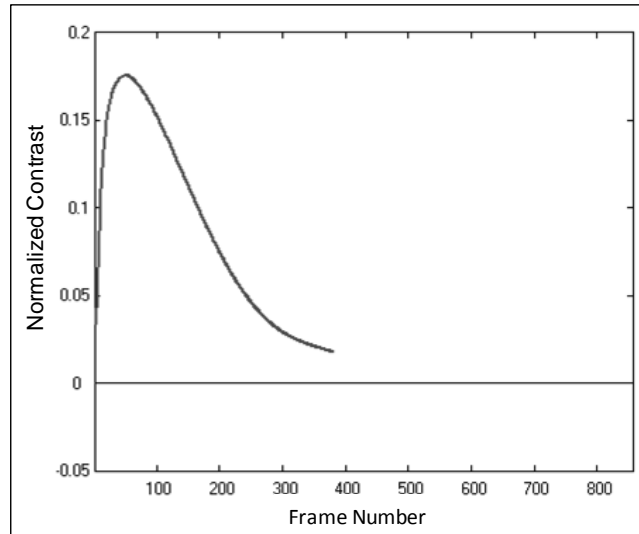


Figure 11: Example of Predicted Contrast Evolution from a Flat Bottom Hole

Figure 13 shows the main interface window of the IR Contrast application with the three contrast evolutions. The differences between the measured data and the simulation are calculated and are indicated in the lower right of the application window. Numbers in black are based on the calculations on the raw contrast evolution. Numbers in red are based on the calculations of the filtered contrast evolution. Numbers in purple relate to the predicted contrast evolution.

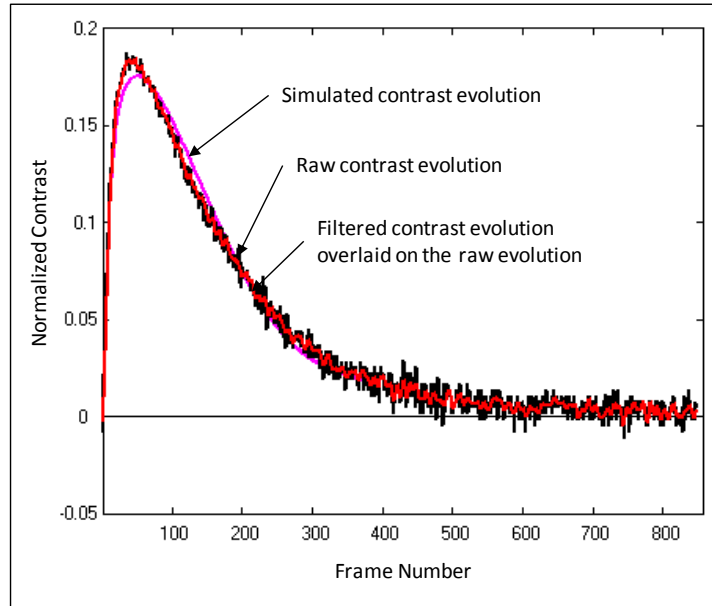


Figure 12: Three Contrast Evolutions (Raw, Filtered and Prediction) Overlaid for Comparison

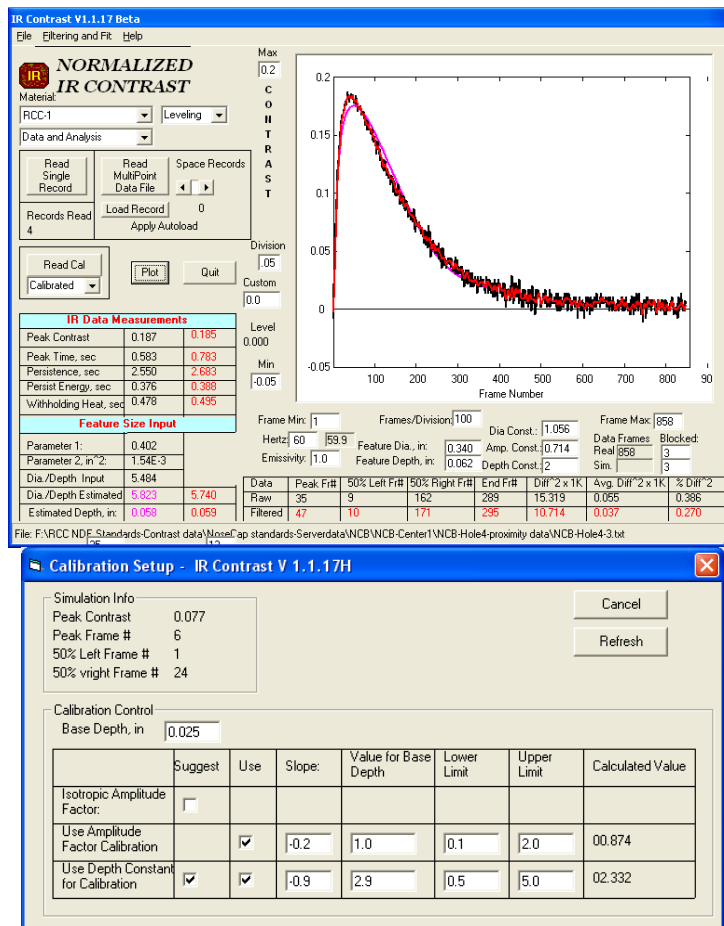


Figure 13: Main Interface for IR Contrast Application with the Three Evolutions and the Calibration Set-up Window

12. Half-max Width Estimation

The width of the indications can be directly measured from the IR data frame that provides the peak in the intensity. The pixel intensities along a line drawn across the linear indication or through the center of a circular indication are plotted against the pixel position. The pixel coordinates at 50 percent of the peak intensity on the right and left of the peak intensity location are located. Pixels between the left 50 percent peak and right 50 percent peak are counted and converted to length by multiplying by the pixel size on the part to obtain an approximate measure of the anomaly width. This technique is called the half-max width measurement technique. See Fig. 14. The technique can be applied to normalized evolutions obtained by subtracting the pre-flash pixel intensity. Also, the choice of frame for the measurement is recommended to be between t_{50L} and t_{peak} . The percent level itself may be different than 50 percent to make the boundary estimations less or more conservative. The half-max approach is limited by the spatial noise. Thus, the half-max intensity to the spatial noise ratio shall be more than 2 to 3 times for meaningful boundary estimation. Resolution of the half-max pixel can be improved by interpolation.

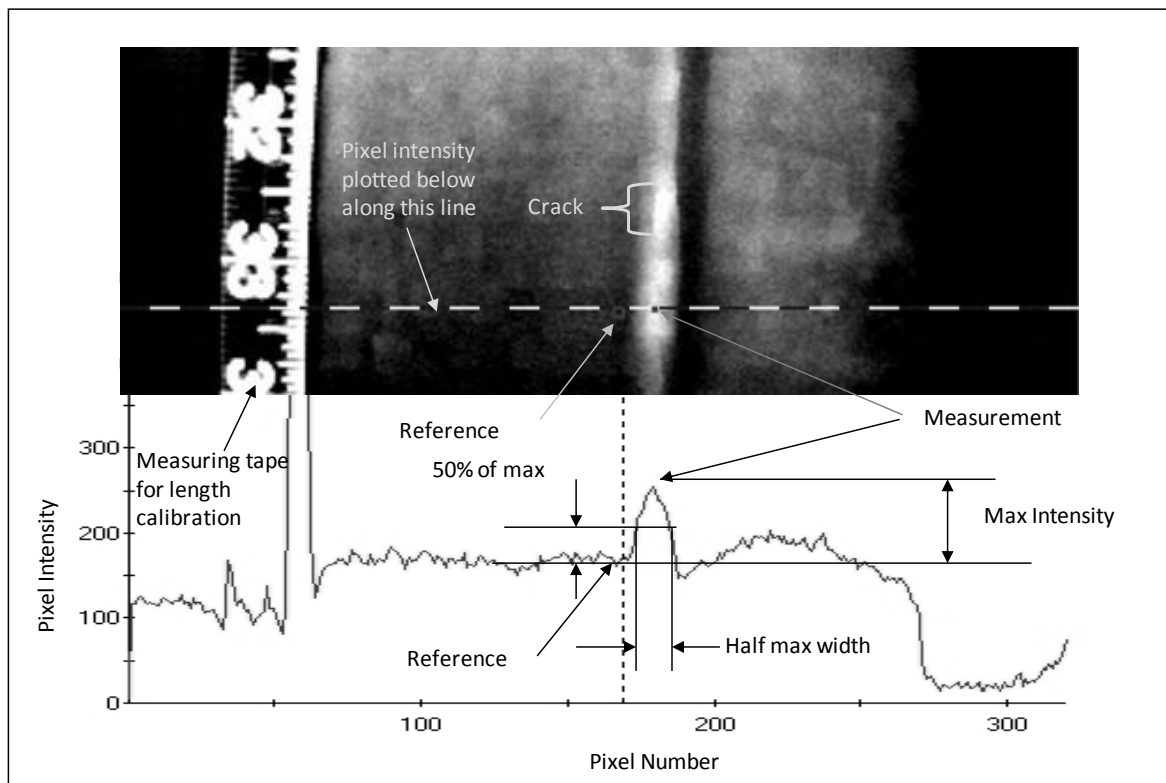


Figure 14: Half-max Width Measurement Technique Width Ratio

In order to compare the EFBH estimation with the observed width, a quantity called the width ratio is introduced. Width Ratio (ψ , psi) is defined as the ratio of the simulation estimation EFBH diameter to the measured half-max width.

$$\psi_{EFBH} = \frac{D_{EFBH}}{w_{hm}} \quad (9)$$

The ψ ratio is designed to be close to 1 for calibration FBH's. If the anomaly is not like a gapping delamination such that the heat is partially conducted or transmitted through the anomaly, then the EFBH estimation is expected to be smaller. Therefore, ψ is hypothesized to correlate to the gap thickness or the degree of heat transmission through the anomaly. The heat transmission through an anomaly occurs due to the contact between the delamination faces, the bridging of material in the delamination gap or due to a very thin air gap. It is hypothesized that a ratio close to 1 on a round delamination implies that the indication is similar to a flat-bottom hole or a gapping delamination. Lower values of the width ratio will have more inaccuracies in the depth assessment due to greater mismatch between shapes of the measured contrast evolution and the simulated contrast evolution.

13. Amplitude Ratio

In order to compare the EFBH estimation with the measured half-max width, a quantity called the amplitude ratio is introduced. Similar to the width ratio, this ratio is intended to evaluate heat transmissivity of the anomaly. If a delamination has an intermittent contact between the faces, the heat will transmit through the delamination. The heat transmission results in lowering of the peak contrast value compared to that from the same size FBH. The overall shape and the peak time are not affected because the normal and lateral transit times remain the same. Here, the half-max width (w_{hm}) is used as a diameter input to the simulation. The depth input to simulation and the amplitude ratio input to the simulation are adjusted to match the measured contrast. The amplitude ratio, denoted by ζ (zeta), is given by,

$$\zeta = \frac{\bar{C}_a^{peak}}{\bar{C}_e^{peak}}, \quad (10)$$

where \bar{C}_e^{peak} is the estimated peak contrast using the half-max width and depth providing a match with the peak time. The amplitude ratio compares the peak contrast (amplitude) of the measured anomaly with the peak contrast of a flat-bottom hole with the same depth and diameter. Thus, the amplitude and width ratio values of a round delamination close to 1 would imply that the anomaly is similar to a FBH. A lower amplitude ratio or width ratio value would imply increased heat transmission due to the material bridging, contact within the anomaly or thin air gap. The material bridging provides adherence of the material above the anomaly but a mere contact may not. Therefore, the amplitude ratio may not always correlate to the material adherence strength.

The width ratio and the amplitude ratio approach are further developed into equivalent uniform gap (attenuation) mapping. The measured signal can be analyzed to provide the

size and depth of an equivalent FBH or the size and depth of a uniform equivalent gap. In this approach the gap thickness can be estimated within limitations.

14. Calibration Steps in the IR Contrast Application

Calibration steps for the IR contrast application are provided in the appendix.

15. Calibration Curves for RCC

RCC is a three layer material with outer layers made from SiC and the middle layer made from plies of carbon-carbon i.e. carbon fibers and carbon matrix. Consider a round FBH or a round void-like anomaly. The diffusivity that controls the contrast evolution is dictated by the location and direction of the dominant heat flow that starts from the measurement ROI and passes towards the edge of the anomaly as well as by the (normal) heat flow from the reference ROI. The heat flow (direction and flux) changes with the time and the effective diffusivity experienced by such heat flow changes with direction and time. The approximate values of effective diffusivity as a function of depth of the flaw should be known before the calibration curves can be established. Here we choose two sets of flat-bottom holes. One set has a depth at a shallow (low) depth of interest and the other is at the deeper (high) depth of interest. It is not necessary to know the exact effective diffusivity in order to establish the calibration curve. It is important, however, to assign a reasonable estimate of the diffusivity to the low depth holes. Using the chosen diffusivity, the simulated contrast evolutions of the low depth holes are obtained and used to establish the diameter constant and amplitude constant. The low (or high) depth can be chosen to be the base depth. Let us choose the low depth as the base depth for the following plots. The RCC calibration standard D2 with high depth (0.050 inch) holes is shown in Fig. 15. The calibration curves obtained from the low depth (0.025 inch) holes of RCC standard D1 are shown in Fig. 16.

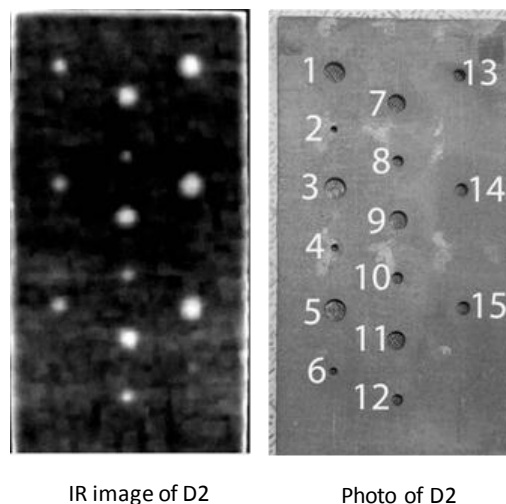


Figure 15: Images of Calibration Standard D2

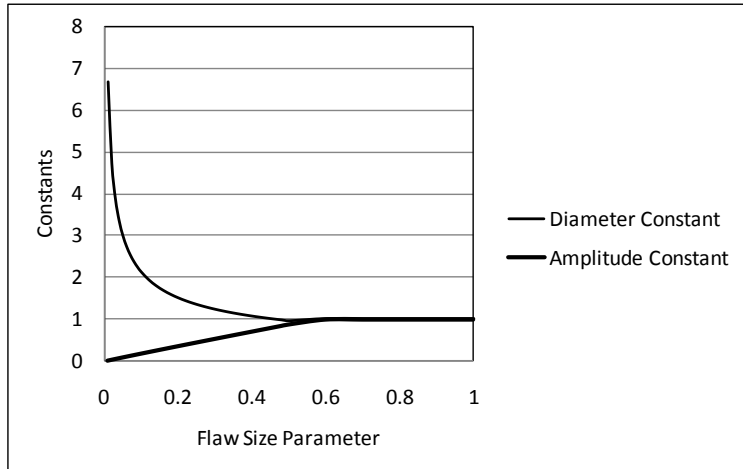


Figure 16: Calibration Curve from Base Depth Holes

The high depth hole contrast evolutions should be used and a diffusivity value is chosen to provide about the same diameter constant to the flaw size parameter relationship as the low depth contrast evolutions.

Figure 17 provides a plot of the depth constant calibration obtained for the calibration standards D1 and D2.

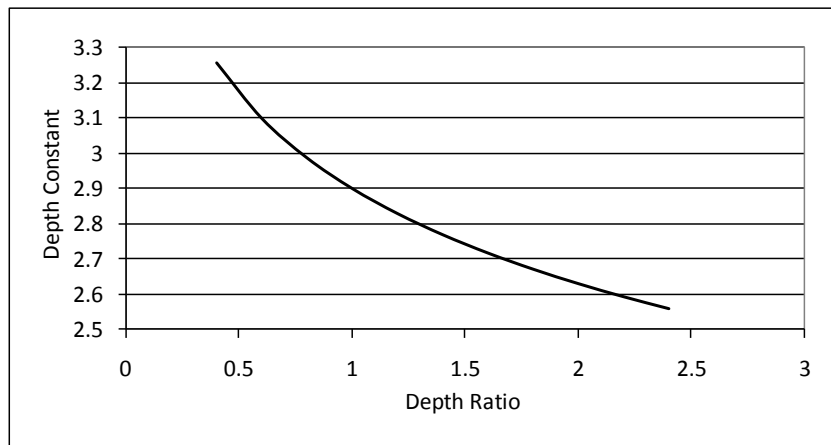


Figure 17: Depth Constant versus the Depth Ratio

The amplitude constant may be depth dependent, too. Figure 18 shows the plot of the amplitude factor calibration obtained for the calibration standards D1 and D2.

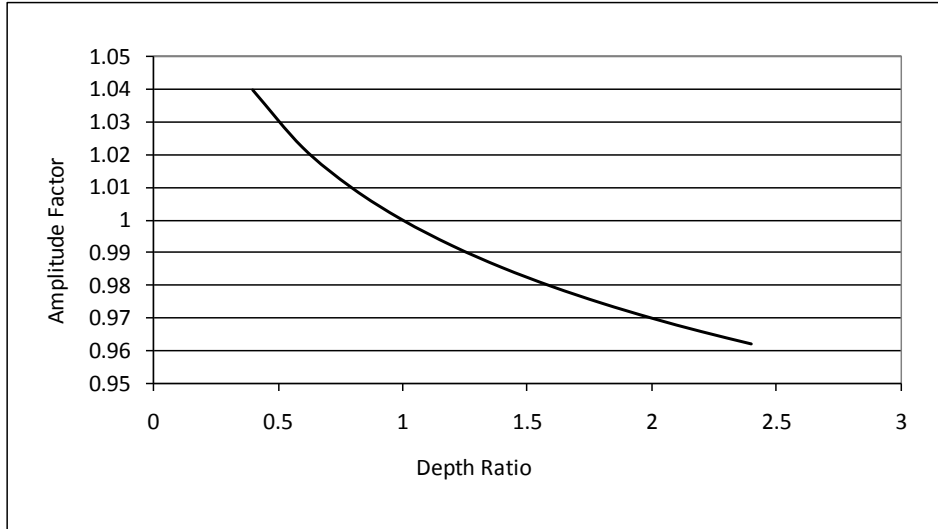


Figure 18: Amplitude Factor versus the Depth Ratio

Results of the calibration as a depth prediction on calibration standards D1 and D2 are shown in Fig. 19.

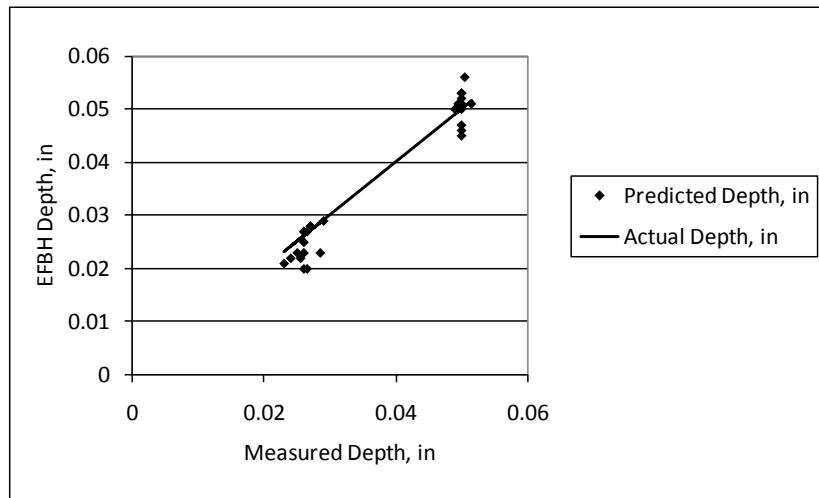


Figure 19: Results of Depth Calibration on RCC Standard D1 (0.025 in deep holes) and D2 (0.050 in deep holes)

Results of the calibration as a diameter prediction are shown in Fig. 20.

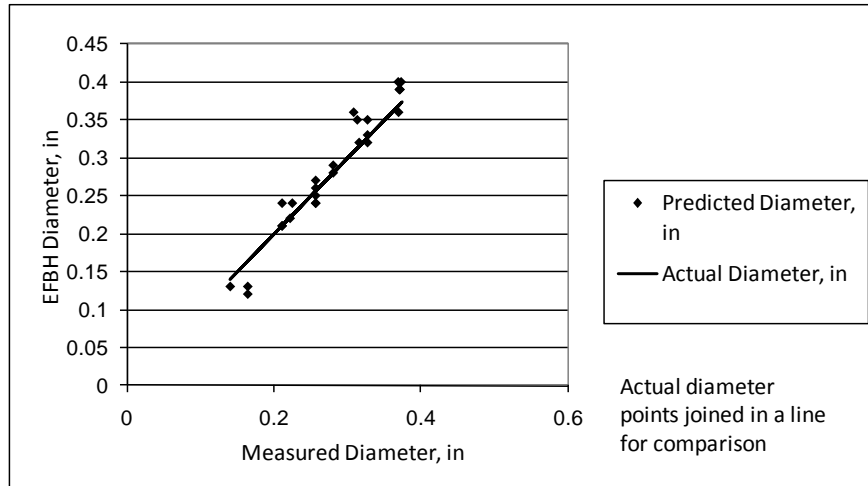


Figure 20: Results of Diameter Calibration on RCC Standard D1 (0.025 in deep holes) and D2 (0.050 in deep holes)

16. Calibration for Specified Attenuation ($\% \mu$) for a Thin Delamination

It is assumed that an air gap exists in the delamination. The heat transmits through the air gap. Thin gaps transmit heat by air conduction. Thick gaps transmit heat by convection. The radiative heat transfer is mostly independent of the gap thickness and is not a major contributor to the heat transmission. Higher contact pressure at the gap interface provides larger contact area. Therefore, the contact pressure affects the rate of heat conduction.

As the energy is transmitted through the gap, the registered peak amplitude is reduced compared to the amplitude from a corresponding FBH. The calibration curves for a uniform thin gap are different from that of a corresponding FBH. Ideally, physical reference standards with known and uniform gaps shall be fabricated to establish the calibration curves for known gaps. However, using simulation, it can be shown that a gap of less than 0.010 inch is needed to reduce the contrast amplitude significantly. While very thin gaps can be modeled in the simulation, it may be impractical to create controlled gaps that are less than 0.001 inch in thickness to study the effect of gap thickness on the contrast evolution.

An alternate approximate approach is to use a ThermoCalc (or other) simulation. In the ThermoCalc simulation, we choose many void widths at the same low (base) depth. We choose a different gap thickness for each run. We choose a large gap thickness (0.150 in) to represent the case of a FBH. We choose several other values with the lowest gap thickness at about 0.0005 in. We calculate the peak time ratio and the peak amplitude ratio with respect to the peak time and amplitude of the FBH. The peak time ratio is plotted against peak amplitude ratio for each hole with each gap thickness. Here we choose a desired amplitude attenuation level e.g. 30 percent. The case study (Sec. 20) indicates the attenuation value from 0 percent to approximately 50 percent on the chosen sample. From the plot, we read the value of the peak time ratio for the chosen amplitude

ratio. We create a table of the peak time ratio for the given gap size. We use the IR Contrast application simulated contrast evolution (in calibration mode) to note the peak amplitude and peak time for each void width. We compute the 30 percent attenuation amplitude by multiplying by 0.7 (1.0 minus peak amplitude ratio). We calculate the corresponding peak frame by multiplying the FBH peak frame (IR Contrast simulation) by the peak time ratio. Now we choose the “un-calibrated” mode to input trial values for the calibration constants that provide the best match with the calculated peak frame and peak amplitude.

The real delaminations may have thin gaps and the contrast evolution is attenuated. The relationship between the peak time and peak contrast can be studied by using ThermoCalc simulation for many void thicknesses that range from very thin (0.0005 in thick) to very thick (e.g. 0.150 in). The thick voids can be considered to be like a flat-bottom hole. The contrast evolutions for the FBH’s of various sizes can be used as the basis to compute the peak contrast (amplitude) ratio and the peak time ratio for the corresponding hole widths for each gap thickness. Here, we make an assumption that the ThermoCalc simulation can provide acceptable correlation between the peak contrast ratio and the peak time ratio for a material with known properties. See Fig. 21.

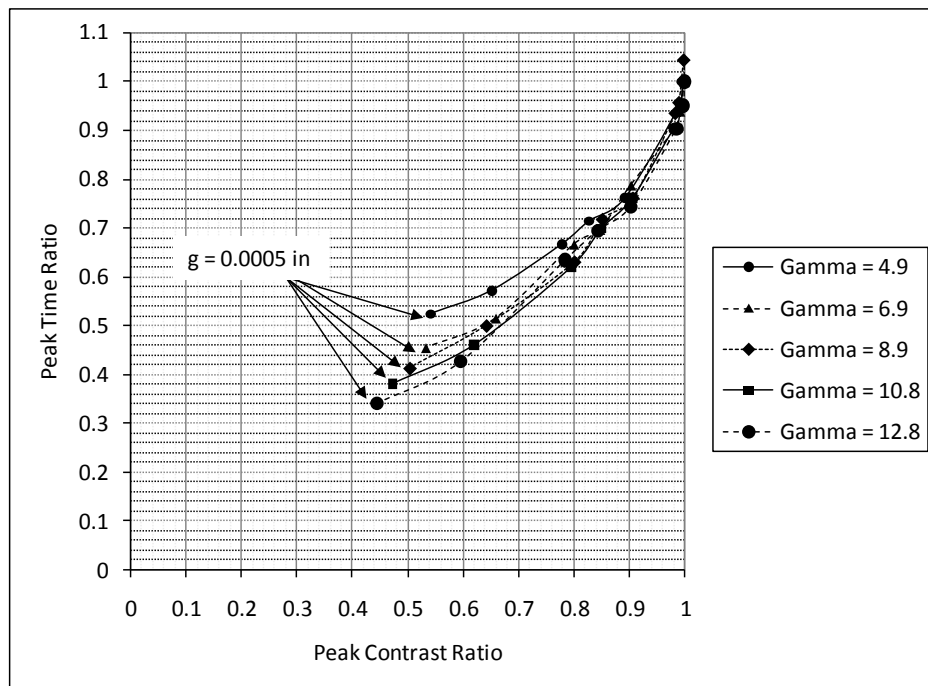


Figure 21: An Example of the Relationship between Peak Time Ratio and Peak Contrast Ratio Based on ThermoCalc Simulation for a void depth of 0.040 in.

Using the above results we can establish a correlation between the gamma (void width divided by void depth) and the peak time ratio for a chosen attenuation in the simulated peak contrast. The fifty percent attenuation corresponds to an air gap thickness of approximately 0.001 in. The attenuation is similar to the amplitude ratio ζ (zeta). While the attenuation is used to compare the peak contrasts of the simulated evolutions,

amplitude ratio is used to compare the peak contrast of the actual evolution with the peak contrast of the simulated evolution.

<i>Void Width, in</i>	<i>Gamma</i>	<i>Peak Time Ratio for 50 Percent Attenuation</i>
0.512	12.8	0.34
0.433	10.8	0.39
0.354	8.9	0.41
0.276	6.9	0.44
0.197	4.9	0.51

Table 1: An Example of Correlation between Gamma and the Peak Time Ratio at Chosen Depth of 0.040 in.

The data in Table 1 can be used to generate the calibration curves for the chosen attenuation. First, the calibration curve (Mode: calibrated) is loaded for the FBH (0 percent attenuation). For each void width and depth, the peak time and the peak amplitude should be determined. Then the mode of the software should be changed to “un-calibrated”. Next, the attenuated amplitude and the peak frame from the corresponding ratios are computed. The diameter and amplitude constants can be determined by trial-and-error. The diameter constant is altered to match the peak time followed by the change in the amplitude constant to match the amplitude.

17. Calibration Curves for Contrast Attenuation

Figure 22 provides an example of calibration curves for no attenuation (FBH) and with 30 percent and 50 percent attenuation.

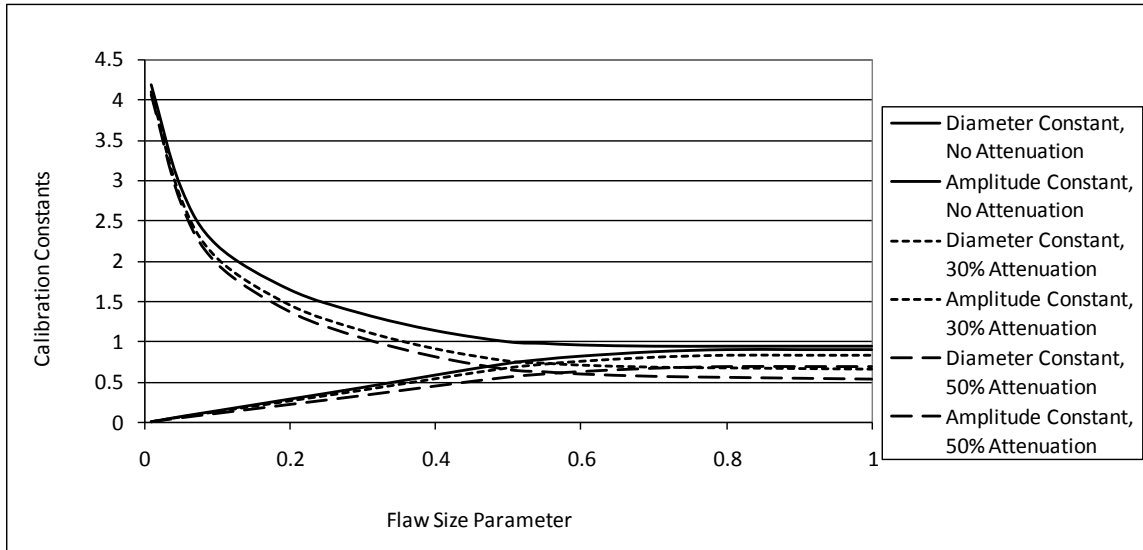


Figure 22: An Example of Calibration Curves for No Attenuation, 30 Percent Attenuation and 50 Percent Attenuation

Seventy percent attenuation calibration curves can be calculated by extrapolating previous curves. The corresponding calibration curves are shown in Fig. 23.

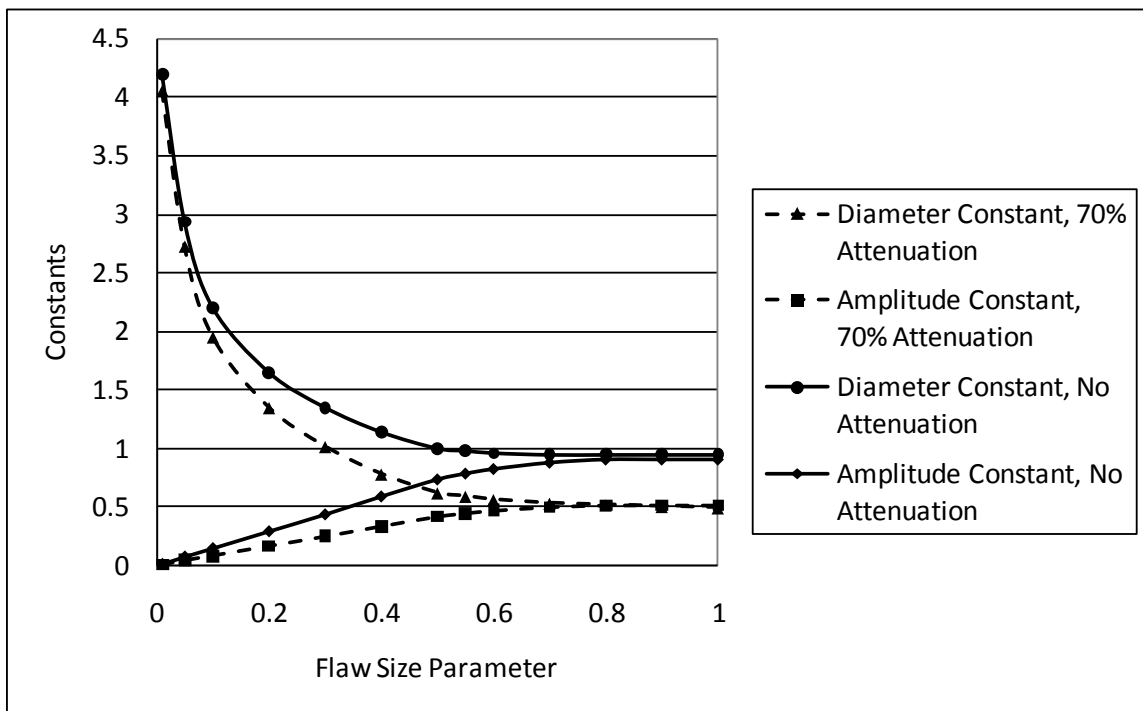


Figure 23: Seventy Percent Attenuation Calibration Curves Estimated by Extrapolating Calibration Curves from Fig. 22

18. Contrast Maps for the Attenuated Calibrations

Figure 24 shows an example of a map of the peak contrast and peak time for flat-bottom holes in RCC. The map is also known as the contrast map. The map indicates the IR Contrast prediction region. At the upper left corner and lower right corner the prediction is not accurate in terms of the diameter. Also, the low amplitude evolutions have higher error in the prediction.

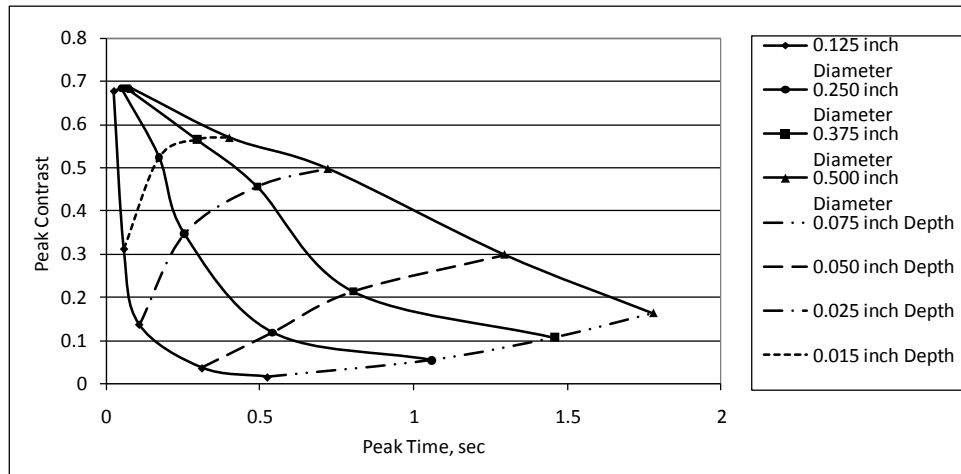


Figure 24: Peak Contrast versus Peak Time Contrast Map for 0 Percent Attenuation (EFBH)

Figure 25 shows an example of a map of the peak contrast and peak time for uniform round thin gaps with 50 percent attenuation in RCC. For thin gaps with 50 percent attenuation, the contrast map indicates much lower peak contrast and peak times. The contrast application can choose FBH calibration or the percent attenuation calibration. When finding a simulation match on the contrast evolutions from a FBH, the percent attenuation calibration may not be able to find a match. Similarly, when finding a simulation match on contrast evolutions from thin delaminations, the FBH calibration may not be able to find a match. The degree of match can be viewed as contrast plots and quantified as the summation of the square of the difference over a range of chosen frames. It is postulated that the 50 percent attenuation is a good approximation for gaps of the order of 0.001 in based on the simulation data from Fig. 21. The map indicates severe contrast attenuation at 0.5 sec for the 50 percent attenuation.

Figure 25 indicates that compared to the contrast map for the FBH's, the near surface delaminations attenuate relatively less than the deeper delaminations. The air-gap at the delamination is similar to a contact resistance or a thermal mismatch factor between layers. The thermal mismatch factor between two layers is based on the ratio of effusivities of the two materials. The thermal mismatch between the top layer and the next layer may vary periodically along the interface in a laminated structure which uses fabric and matrix. Similarly, the emissivity and diffusivity of the top layer may vary periodically along the surface. The variation in diffusivity, emissivity and mismatch factor between the top two layers as well as the surface texture or roughness pattern is

referred to as the surface/near surface thermal texture. Figure 25 implies that a hot spot in the IR image of the surface texture would provide an early peak. Here, we assume that measurement ROI size is smaller than or equal to the width of the hot spot. Similarly, a cold spot should provide a negative peak in the contrast profile. Thus, in detection of delaminations, it is important to properly interpret the early time peaks as possibly due to surface texture. These indications may superimpose on the signal from shallow delaminations reducing resolution in evaluating shallow delaminations.

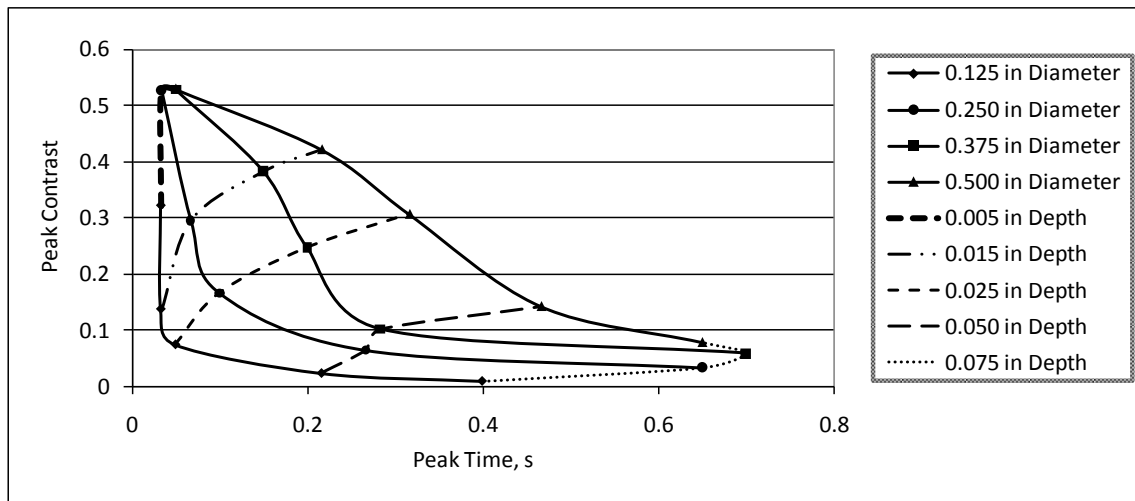


Figure 25: Peak Contrast versus Peak Time Map for 50 Percent Attenuation (EUG)

For long indications the EFBH or EUG diameter estimations are higher than the actual width due to the length to width aspect ratio being greater than 1. The effect can be studied on a slot standard. Figure 26 shows a slot standard and IR image of holes 3, 4 and 5. The figure also illustrates the half-max boundary detection. The half-max boundary closely matches the actual vertical edges of the three anomalies.

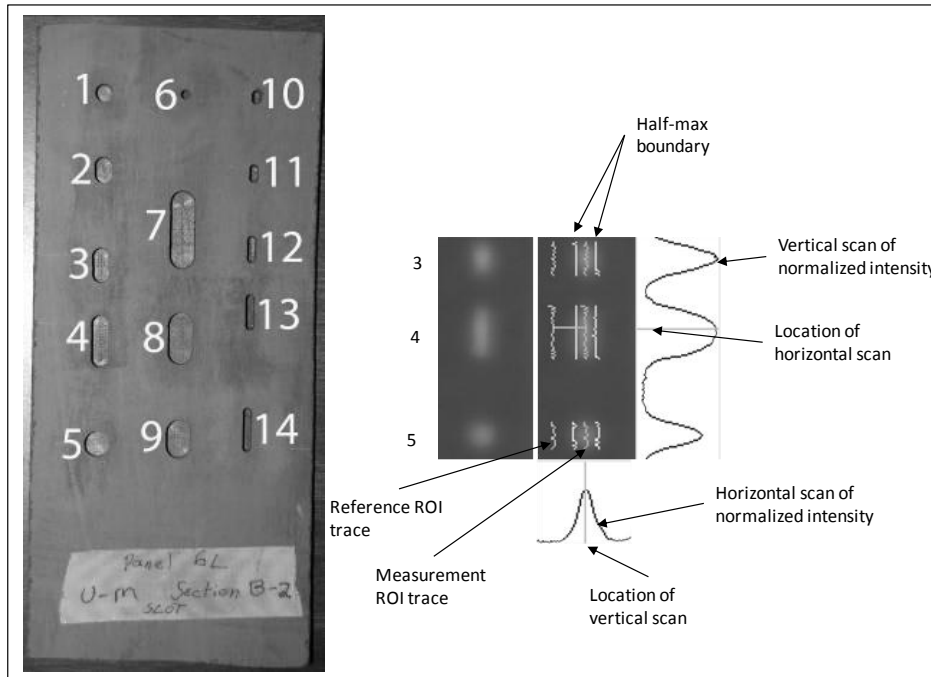


Figure 26: Slot Specimen, IR Image at 0.67 sec of Hole 3 (Top), Hole 4 (Middle) and Hole 5 (Bottom) and Their Half-Max Vertical Boundary

Figure 27 shows that on a long 0.25 inch wide slot (#4), EFBH estimations are 60 percent wider than the actual but on the round hole, as expected, the prediction is close to the actual diameter.

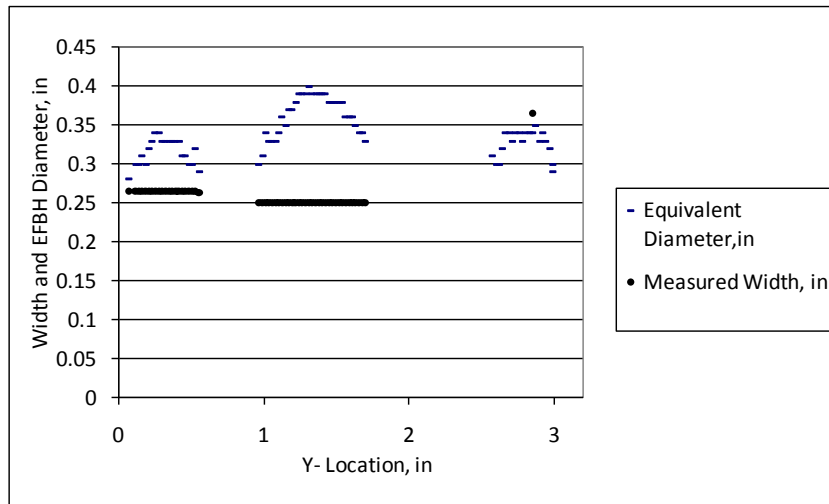


Figure 27: Comparison of Actual Width with Predicted EFBH Diameters for Holes 3, 4 and 5 (File: Right threeslots.xls)

If the data contains only long indications, it may be advantageous to set up calibration on long slot (aspect ratio >3) standards using the width in place of the diameter. In this

situation, correction for the length effect will not be needed for most of the length of the indication except near the ends.

19. Similarities and Differences between Flash Thermography IR Contrast Analysis and Ultrasonic Pulse Echo Analysis

It is important to point out similarities and differences between the pulse-echo ultrasonic A-scan analysis and the contrast evolution analysis. The IR Contrast algorithm is used to analyze delamination-like anomalies. The IR Contrast concept is similar to flaw sizing in ultrasonic inspection of wrought metal. In the ultrasonic technique, usually a plate of wrought metal is inspected for internal separations. The part may be immersed in water along with the ultrasonic transducer.

A longitudinal ultrasonic pulse is triggered at the transducer and is transmitted through water to the part where a portion of the ultrasonic pulse is reflected and a portion is transmitted into the part. The pulse reflects off the anomaly and some of the reflected pulse energy, after passing through the water-to-metal interface, is received back by the transducer. The ultrasonic instrument provides an A-scan display. The A-scan shows the waveform of the received pulse. The horizontal or X-axis is the time of the waveform. The X-axis can be calibrated in distance of length of the one-way sound-path of the pulse reflections from the top surface of the part. This distance corresponds to the depth of the reflector from the top surface of the part. The beginning portion of the A-scan has the waveform of the initial pulse applied to the transducer. The remaining portion of the A-scan indicates the reflected pulse energy. The reflected pulse amplitude is affected by the depth and size of the reflector.

Flat-bottom hole reference standards are used to calibrate the inspection technique for depth and depth-amplitude correlation. In addition, area-amplitude correlations can also be established externally.

The ultrasonic pulse has a beam width. The aperture and curvature of the transducer influences the beam width. The beam width usually changes with the distance from the transducer. For an unfocused transducer, the aperture primarily controls the amount of energy received. For a focused transducer, both beam width at the reflector and the aperture influence the amount of energy received.

The IR Contrast evolution shows some similarities with the ultrasonic pulse-echo A-scan, especially when the ultrasonic signal is rectified on the positive side and the envelope mode is used. The horizontal axis is time in both cases. The peak time in both cases relates to the depth of the anomaly from the part surface. In the ultrasonic technique, the ultrasound material velocity is used to convert peak time to reflector depth by multiplying the one-way transit time observed in the A-scan by the velocity of ultrasound. In the IR Contrast analysis, material heat diffusivity is primarily used to convert the peak time to depth although width of the contrast envelope (persistence time) also affects this

correlation. Both techniques use flat-bottom hole standards for amplitude/depth calibration. In the ultrasonic technique, the depth amplitude factor calibration can be incorporated in real-time such that the chosen area of the flaw provides the same amplitude at a range of flaw depths. In the IR Contrast analysis, the calibration is applied to a separate simulated contrast evolution. The actual contrast evolution is not altered by the calibration. Similar to the ultrasonics, the area/amplitude correlation is also established for the IR Contrast. Typically, FBH at two depths of interest are chosen.

As the flaw size increases, the amplitude of reflected ultrasonic pulse increases but as the size of the flaw grows comparable to the aperture or the beam width at the flaw, the growth in the amplitude slows and reaches a saturation value. A similar relationship is observed for very high gamma (diameter/depth) flaws in the IR Contrast evolution. The contrast signature is not affected by further increase in the gamma. For elongated flaws, typically the growth in length beyond two times of the width does not increase the IR Contrast peak amplitude significantly for shallow flaws.

Tighter delaminations transmit ultrasound depending upon the amount of contact pressure or bonding. Tighter delaminations conduct heat depending upon the amount of the contact pressure. While thin delaminations can conduct and convect heat, they cannot conduct detectable ultrasound at megahertz frequencies. If there is no contact pressure or bond, very little ultrasound energy is transmitted.

In the ultrasonic pulse-echo technique, a single delamination may register multiple echoes in the A-scan. In the IR Contrast, only one envelope is registered by a single delamination. In the case of multiple delaminations of about the same size that are stacked, only the nearest delamination is detected by both ultrasonics and the flash IR technique. In a special case where a vertical surface crack or cracks connect to a subsurface delamination, two peaks may be observed in the contrast evolution as described in the following case study. The first peak is usually very sharp (short persistence time) and is due to the surface cracks or surface (or near-surface) texture. In graphite-epoxy laminates, the weave pattern of the top layer may provide surface texture. Depending upon the pixel location a sharp peak or a sharp dip may be observed in earlier times.

In ultrasonics, the near surface resolution is limited by the surface roughness, ultrasound wavelength and the beam diameter. In flash thermography, the surface texture reduces near-surface resolution. In order to image the texture satisfactorily, the IR image pixel size should be less than a third of the texture wavelength (or the width of the hot spot or the stripe in the IR image). In order to detect a thin gap sub-surface delamination under the texture, the width of the sub-surface delamination should be more than the texture wavelength and it should not be aligned with the texture.

The second peak has lower amplitude and longer persistence time; and is due to the delamination. In some situations the two peaks may merge into one envelope with only one distinct peak location which is heavily influenced by presence of the crack. Echoes

from vertical cracks are very small in the longitudinal wave pulse-echo ultrasonic inspection compared to the echo from a delamination.

20. Case Study: RCC Joggle Area Test Pieces with Subsurface Delaminations

We analyze an RCC test piece with a linear (along vertical or Y-direction) delamination. Figure 28 shows an IR image of a test piece (6L-2A_25-30y_ss_200P06L004). The two white dots in the center indicate near surface delaminations known as flakes.

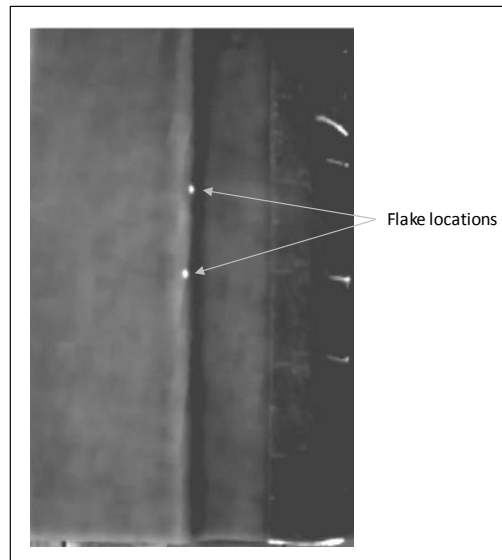


Figure 28: IR Image of RCC Joggle Area Anomaly

Figure 29 shows the half-max boundary in white. The gray line between the left and right half-max boundaries indicates the high intensity locations chosen as the measurement points and the leftmost gray line shows the reference locations. A contrast data file is extracted based on the measurement and reference points and is analyzed by the IR Contrast application for diameter and depth.

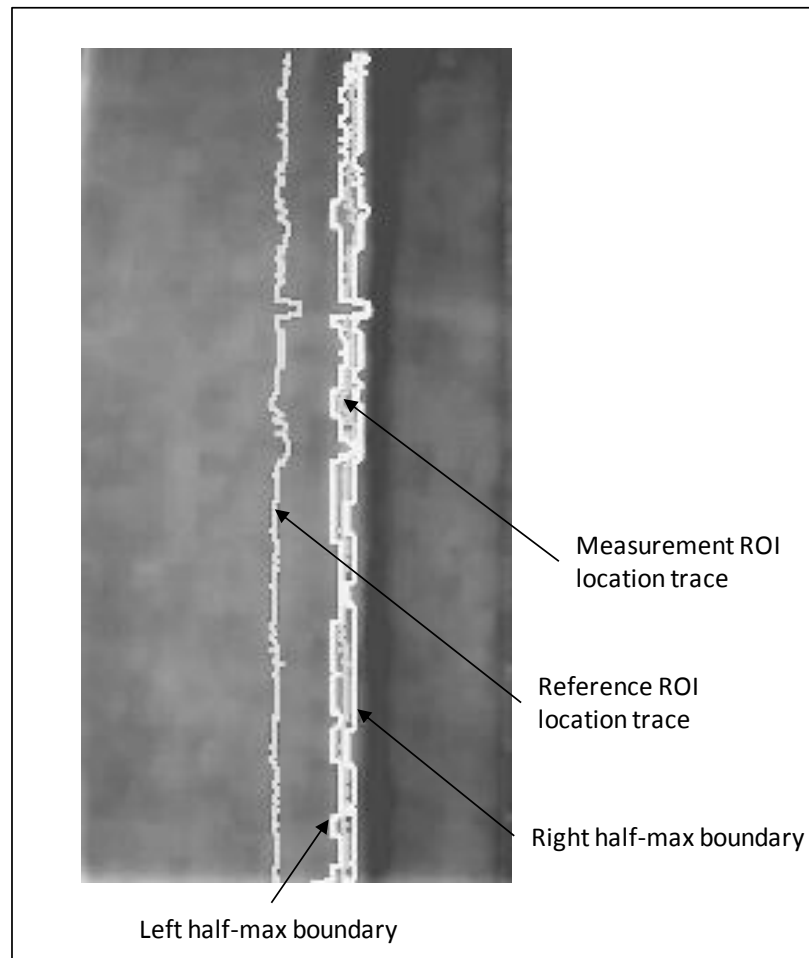


Figure 29: Contrast Extraction Locations and Half-max Boundary

Figure 30 shows a typical contrast evolution at a chosen measurement pair (measurement ROI and corresponding reference ROI) when craze cracks are not present close to the measurement ROI.

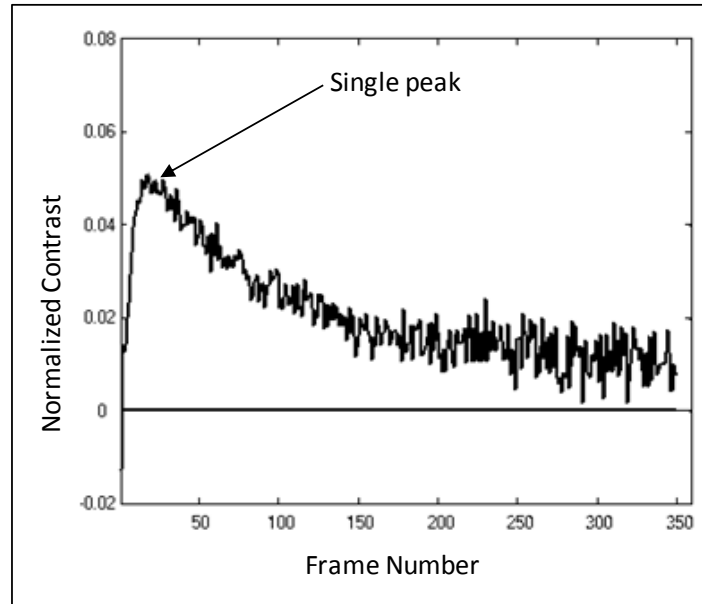


Figure 30: Typical Contrast Evolution without Craze Crack Influence

Figure 31 shows a typical contrast evolution for a chosen measurement pair when craze cracks are present close to the measurement ROI. The initial peak in the evolution is due to the crack, the later peak is due to the delamination. The IR Contrast application allows choice of signal matching either to the initial peak or to the later peak by allowing to block (or blank) the evolution in the initial frames after flash. The IR Contrast technique can assess severity of the cracks as mapped into the EFBH's.

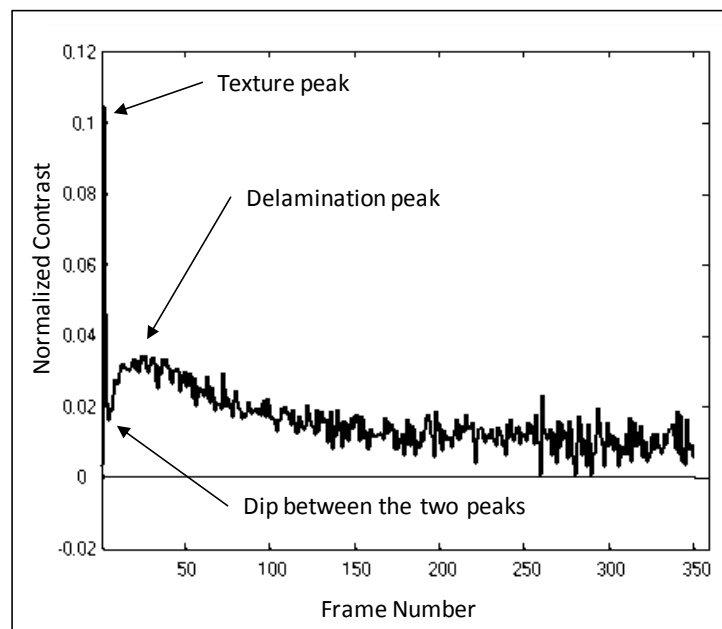


Figure 31: Typical Contrast Evolution with Craze Crack Influence

The craze cracks may be connected to the delamination and the initial and later peaks may get merged as shown in Figs. 32 and 33.

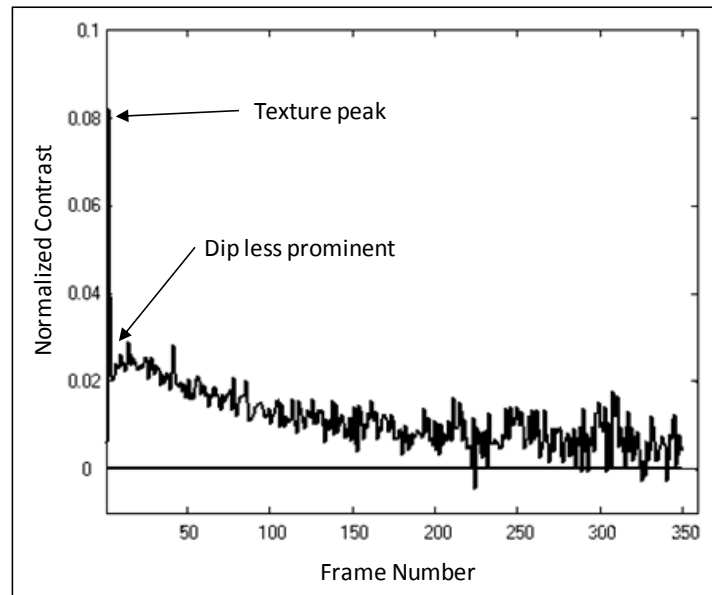


Figure 32: Typical Contrast Evolution with Craze Crack Influence, Second Peak Less Distinct

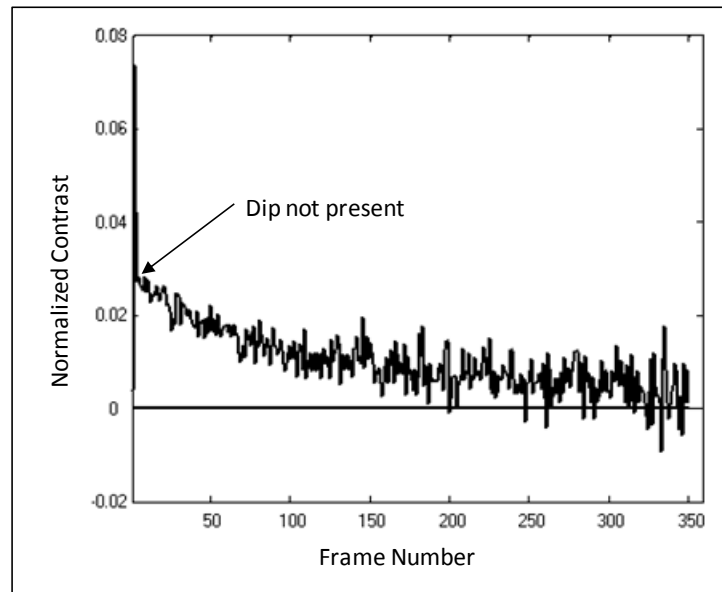


Figure 33: Contrast Evolution with Craze Crack Influence, No Second Peak

Figure 34 shows the peak contrast plot. Two peaks at 1.8 in and 2.8 in are due to flake spots. The peak contrast is strongly related to the local width of the linear anomaly.

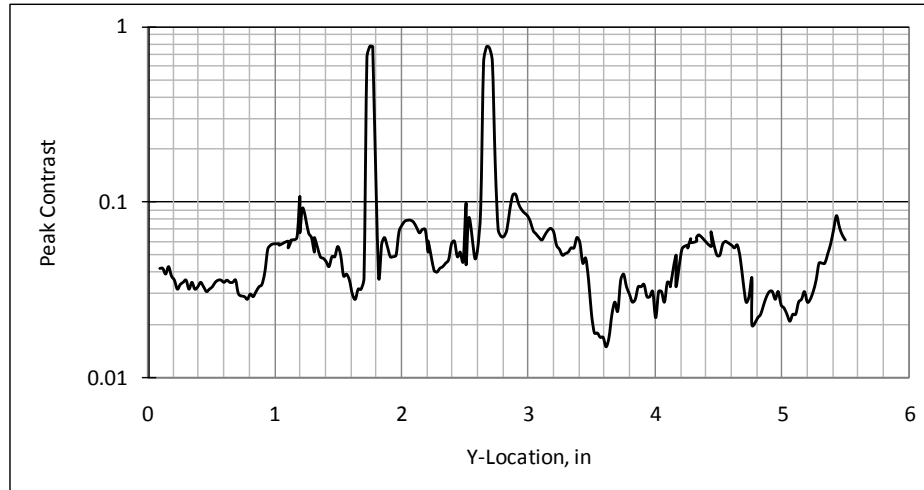


Figure 34: Peak Contrast along the Indication

Figure 35 shows the peak time plot. In most of the region the peak time is less than 0.5 sec. In some locations it is greater than 0.5 sec. The peak time is strongly related to the local depth of the linear anomaly.

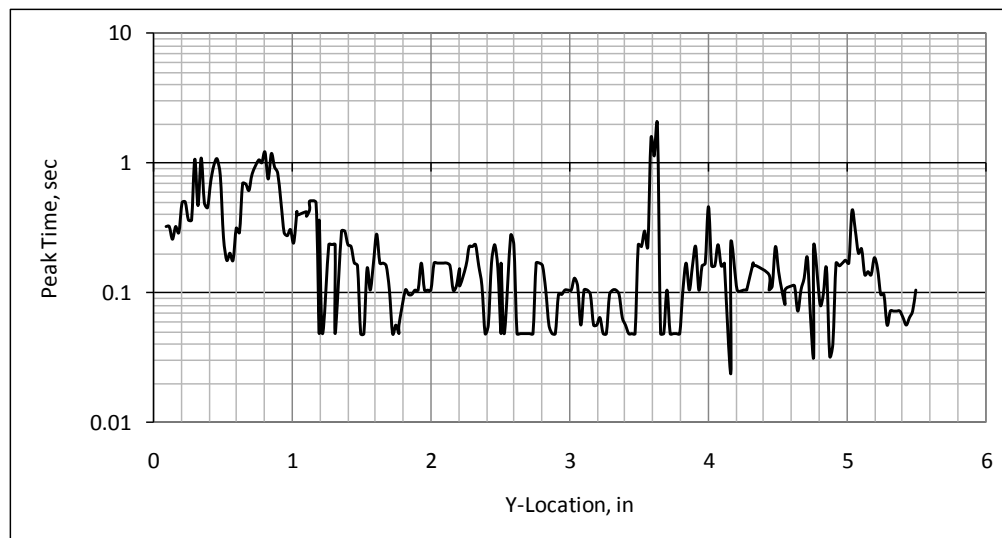


Figure 35: Peak Time along the Indication

Figure 36 shows the persistence energy time. It shows the two flake peaks at 1.8 inch and 2.8 inch. The plot indicates relatively high persistence energy time from 0 in to 1 in. The persistence energy time is strongly related to the local width of the anomaly.

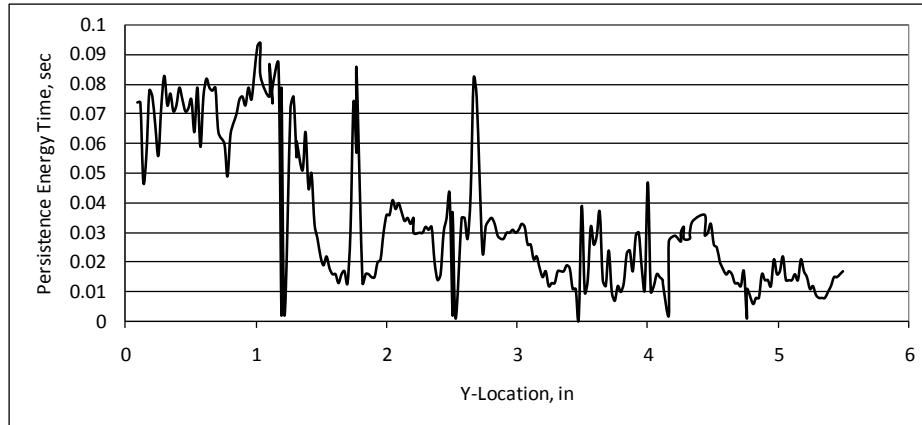


Figure 36: Persistence Energy Time along the Indication

Figure 37 provides IR Contrast and half-max predictions. The IR Contrast and half-max widths seem to provide measurements on the same order of magnitude. The flake indications show lower half-max and higher EFBH diameter, indicating a relatively higher gap thickness. Indications that show higher half-max width and lower EFBH diameter imply that the gaps are thinner (see Fig. 37 at Y-Distance of 2.7 inch).

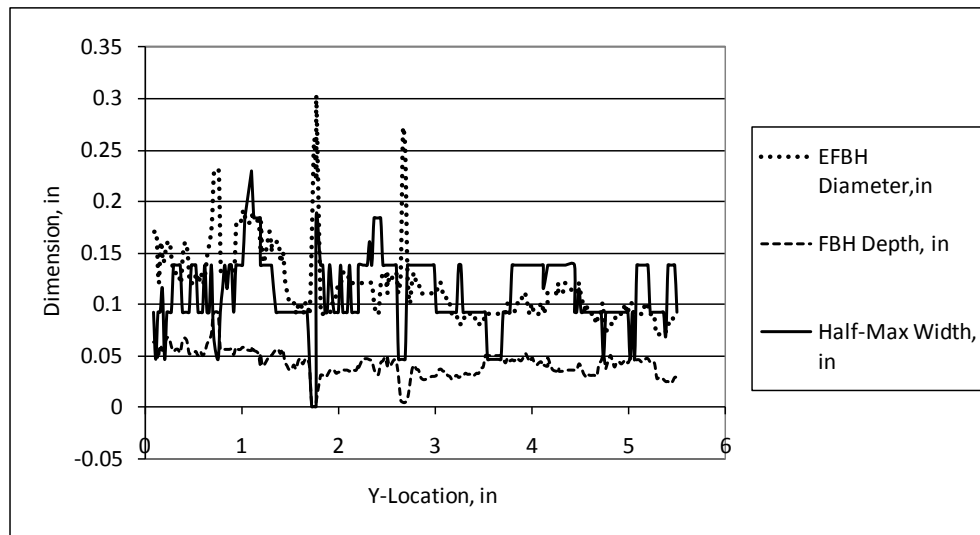


Figure 37: EFBH Diameter, Depth and Half-max Width Estimations

Results of the attenuation contrast analysis with 0 percent, 30 percent and 50 percent attenuation are shown in Figure 38. The depth predictions in the three attenuation analyses are about same. The 50 percent attenuation diameter is about 1.6 times the 0 percent attenuation diameter.

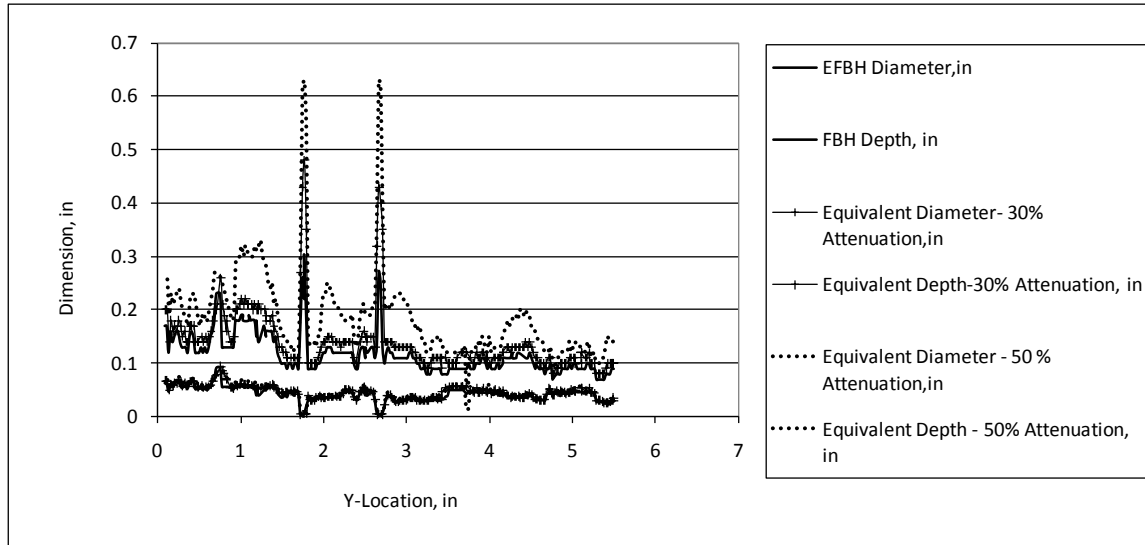


Figure 38: IR Contrast Diameter and Depth Prediction

As expected, the analysis with thinner gaps shows higher diameter estimation. Since the indication is long, the EFBH and attenuation diameters are expected to be approximately two times of actual width. The delamination is not like a flat-bottom hole but is more like a thin gap delamination. We would assume that the delamination is close to 50 percent attenuation (or a gap of about 0.001 in). Therefore, to obtain an approximate estimate of width we divide the EUG diameter by about 1.6 (0.250 inch wide delamination at 0.040 in depth). The comparison is shown in Fig. 39. The EFBH and the adjusted 50 percent attenuation EUG diameter estimations are in good agreement implying EFBH estimations on the long RCC indications may provide comparable estimations to 50 percent attenuation measurements with adjustment for the aspect ratio.

Indications that have about the same value for both the EFBH diameter and the half-max width (or the adjusted 50 percent attenuation width) indicate that the gap thickness assumed in the 50 percent attenuation analysis is applicable. The attenuation analysis is based on use of thermal simulation, assumed delamination depth and expected width of a longitudinal delamination. The EFBH analysis does not use the thermal simulation but assumes a range of delamination depth and width. If results from the EFBH and the attenuation analysis look comparable, one may choose to use EFBH analysis only.

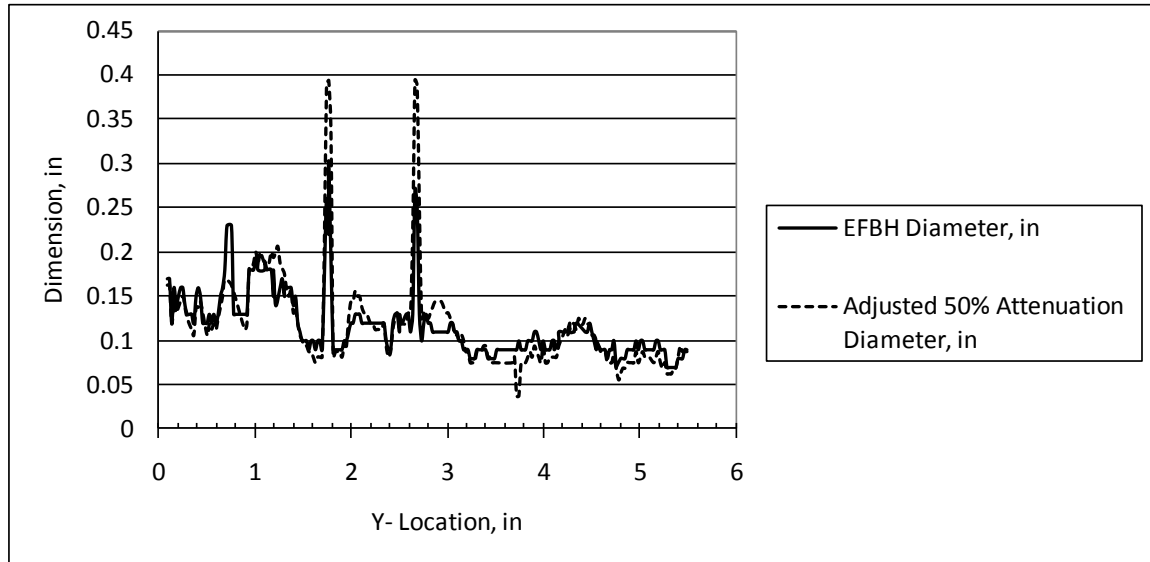


Figure 39: Comparison of EFBH Diameter and Adjusted 50 Percent Attenuation EUG Diameter

Typically the buckling strength across the width of the linear delaminationlike indication would be proportional to the inverse of gamma square. Therefore, a plot of the inverse of gamma square is shown in Figure 40. Low values are expected to indicate lower buckling strength. Correlation of this quantity with the pull strength has not been established.



Figure 40: Inverse of Gamma Square Variation along the Y-Location

Figure 41 shows a plot of the peak product time (Eq. 8a) based on measurements on the simulation fitted contrast evolution and a plot of the EFBH diameter estimation. The shapes of the two plots are similar, indicating a positive correlation.

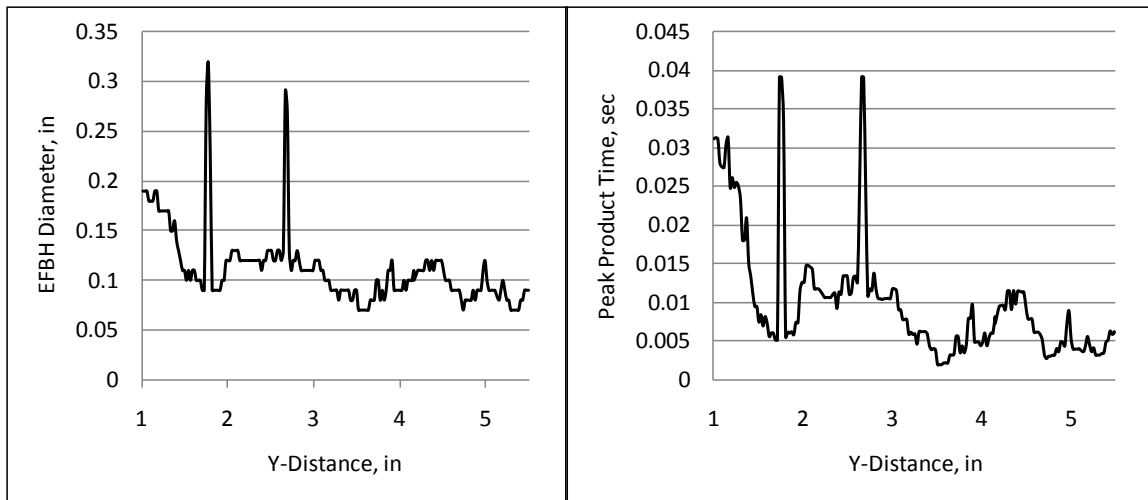


Figure 41: Example of Use of Peak Product Time as a Parameter Related to EFBH/EUG Diameter

Figure 42 shows a plot of the peak time to contrast ratio (Eq. 8b) based on measurements on the simulation fitted contrast evolution and a plot of EFBH depth estimation. The shapes of the two plots are similar indicating a positive correlation. Note that the contrast evolution data in Fig. 41 and 42 was extracted separately. It shows some differences from the rest of the plots in this case study (Fig. 37), suggesting that the parameter values used in the contrast extraction and analysis affect the results.

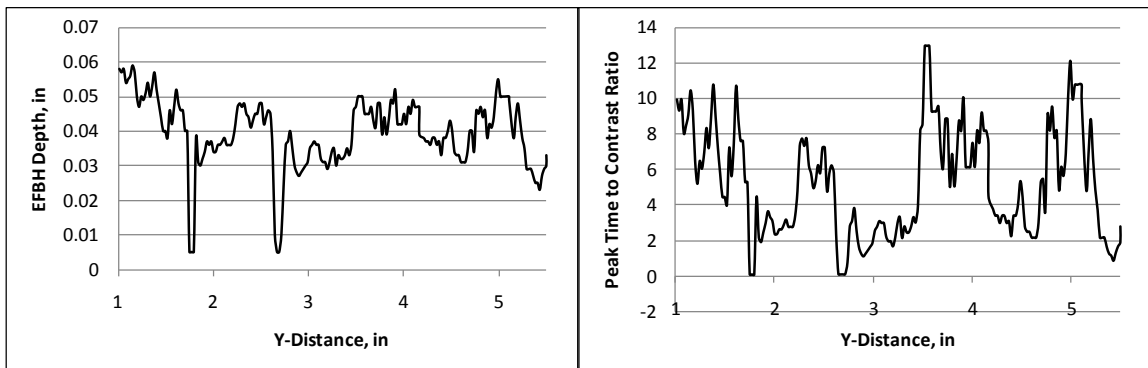


Figure 42: Example of Use of Peak Time to Contrast Ratio as a Parameter Related to EFBH/EUG Depth

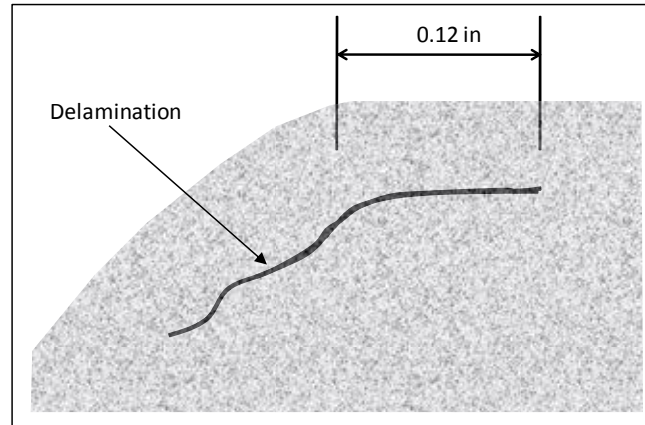


Figure 43: Typical Schematic of Cross Section of the Specimen

Figure 43 shows a schematic of typical microscopic cross section of an RCC specimen. The IR Contrast width estimations seem to match approximately with the width measurements in the aero-surface (horizontal surface) regions. IR Contrast depth estimations are of the same order as indicated by the microscopy section.

The flash thermography response is limited to the horizontal (or aero) surface. The sloping surface receives less flash heat and the IR response is weak in this area. Thus, the half-max and IR Contrast EFBH or EUG diameter measurements should be compared to the microscopy measurement of delamination width (e.g. 0.12 inch) which is under the aero-surface. The half-max, EFBH and adjusted 50 percent attenuation EUG diameters approximately compare with the microscopy measurements. It is better to measure both half-max and the EFBH diameter or half-max width and the adjusted 50 percent attenuation EUG diameter to corroborate the measurements to increase confidence in these measurements. Both the half-max and EFBH (or EUG) diameter measurements provide error in the estimation by themselves due to the fact that the real delaminations are not like flat-bottom holes or uniform gaps. The gap in a real delamination usually tapers towards its boundary. Some delaminations in RCC also have surface (or craze) cracks over the delamination. The craze cracks are open to the surface and extend towards the delamination. Estimating the delamination width by analyzing the signal in time (IR Contrast evolution) and in space (half-max boundary) provides higher confidence in the estimations.

The half-max estimation of the width is considered to be the primary estimation of the width. The EFBH (or EUG) diameter estimations are considered to be secondary for measurement of the width, as these have larger influence from the delamination gap. For uniform gaps, the influence of gap thickness can be accounted for in the EFBH (or EUG) analysis and the EFBH (or EUG) estimate can be fairly accurate. Width ratio, ψ is considered to be a measure of the average gap thickness as it is obtained by normalizing the EFBH diameter by dividing it by the half-max width. Unfortunately, the real delaminations have the thickest gap close to the center and the gap tapers towards the edge very gradually. The tapering delamination boundary cannot be accurately determined solely by the current half-max or the EFBH analysis. The concept of

attenuation (coefficient μ) has been defined for a uniform gap which has a definite boundary that can be assessed by both the half-max and EFBH analyses. The tapering delamination does not have a uniform gap but it has an “effective attenuation” value that is assumed in the IR Contrast analysis corresponding to an “effective or average gap”. Using the ThermoCalc simulation, we can approximately correlate the uniform gap thickness with the attenuation and assume that the correlation is conceptually valid for localized measurement of the gap thickness in a nonuniform tapering gap. In other words, we assume that portions of the tapering gap with higher thickness have higher influence on the amplitude of the contrast evolution than the areas with thinner gap that are further away from the measurement ROI.

Consider a delamination with a gap that tapers uniformly from the center with an attenuation equal to 50 percent to a gap with an attenuation of 90 percent at a certain radial distance from the center. Finally, almost 100 percent attenuation is reached at even larger radial distance. The area of delamination with attenuation between 90 percent and 100 percent would not contribute significantly to the contrast evolution extracted at the optimum measurement ROI due to its greater distance from measurement ROI and higher attenuation value. Thus, there is a limit on the fractional range of attenuation (e.g. $\Delta\mu_{\text{lim}} = 0.5$), that influences the contrast evolution primarily depending upon the gap thickness and the gap thickness slope (dg/dw) profile in a tapering delamination. The fractional range on the attenuation is defined as,

$$\Delta\mu_{\text{lim}} = (\mu_{\text{edge}} - \mu_{\text{min}}) / (1 - \mu_{\text{min}}) \quad (11)$$

Here, the μ_{min} is the attenuation corresponding to the optimum location of the measurement ROI, which in most circumstances also corresponds to the location of the maximum gap and therefore has a relatively minimum value. μ_{edge} is the attenuation at a location close to the half-max boundary and defines the edge of the primary region of measurement. In some situations, where there is an abrupt change in the attenuation, for example, from 90 percent attenuation to 100 percent attenuation in a chosen width direction due to abrupt termination of the delamination gap, the edge location determined by the above condition is likely to be very close to the half-max edge location. The half-max edge in turn is also likely to be very close to the physical edge of the delamination. In situations where the delamination tapers, for example, from 90 percent attenuation to 100 percent attenuation on a relatively long distance, both the half-max width and EFBH diameter based on the single optimum measurement ROI do not provide measurement of the width that also includes the region with the very thin gap (e.g. 90 percent to 100 percent attenuation) that occurs close to the outer edge of the delamination. However, these measurements are useful as a measure of the portion of delamination that contributes the highest to the IR Contrast evolution of the optimum measurement ROI and relate to the average (or effective) gap thickness of the delamination within a region bounded by the half-max boundary.

Also, based on the known relationship between the half-max boundary and the actual tapering delamination boundary, the delamination boundary may be estimated by adding appropriate correction to the half-max boundary. A correlation between the width ratio (ψ) and the average gap thickness may be established based on the destructive microscopy data obtained after the IR data acquisition. It is easy to measure the maximum gap thickness from the microscopy images rather than the average gap within the half-max span. The maximum gap thickness bears a correlation to the average gap thickness. Therefore, a monotonic correlation between the maximum gap thickness and the width ratio can be established using the microscopy data. The correlation then can be used to assess the gap thickness of similar delaminations by analysis of the IR data.

An example of experimental data of width ratio (EFBH diameter/half-max width) versus the actual gap in the RCC joggle specimens similar to that shown in Fig.43 is provided in Fig. 44. The data was taken on RCC specimens 2637, 2639, 2642 and 2686. Interpolation within pixels was used for the half-max width estimation. There are many unaccounted factors that cause variability in the data. During the IR data acquisition, a cover (T-seal) was present over the sloping surface. This adds a small variability in the contrast evolutions especially if the delaminations extend under the sloping surface. The half-max width measurement is also less accurate due to the presence of the cover. Moreover, some specimens had surface cracks which affected the contrast evolutions.

After the IR data acquisition, the specimens were sectioned to enable microscopy measurements of the delamination gaps at the selected locations. The measurement ROI locations in the IR data were matched to the corresponding microscopy section locations and the error in the match is estimated to be at least a couple of pixels (0.023 in/pixel). The gap thickness varies along the width (span) direction making it difficult to assign a single effective gap thickness from the microscopy measurements. There is a certain amount of error in locating the gap measurement locations close to the measurement ROI. The data does imply the expected correlation between the width ratio and the delamination gap. A width ratio of 1 implies a very thin gap (e.g. 0.0005 in to 0.001 in). There is an upper limit for the width ratio (e.g. 3) corresponding to the gap simulating the flat-bottom slot. At this limit the slope $d\psi/dg$ becomes zero. Fig. 44 provides some evidence towards such a limit.

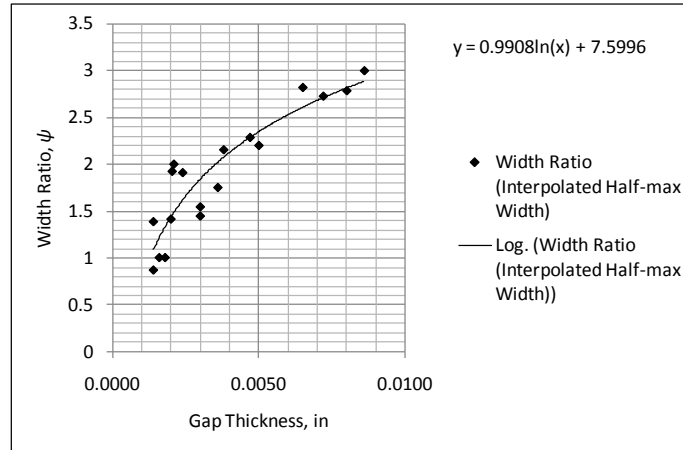


Figure 44: Experimental Data of Measured Gap Thickness versus the Width Ratio on Linear Indications

The width ratio to gap thickness correlation validates the IR Contrast/half-max analysis to characterize the delamination depth, size (width and length) and gap thickness within certain limitations. The width ratio is defined between the equivalent diameter and the half-max width. However, the EUG diameter, gamma, peak product time, persistence energy time, withholding heat time, peak contrast, and persistence time are also strongly related to the equivalent diameter as demonstrated by similarities in shapes of these scans. (See Figs. 34, 36, 37, 39 and 41.) Thus, in the width ratio, EFBH diameter may be substituted by any of the above quantities to define a different gap correlation parameter and establish correlation of the chosen parameter (defined as the ratio with respect to an appropriate power of the half-max width) with the gap thickness. This approach can also be demonstrated by simulation.

An example of the simulation results is shown in Fig. 45. The data is the same as that used in generating Fig. 21. The simulation was done on uniform square voids. A gap correlation parameter is defined as the peak product time divided by the width^{2.3}. Figure 45 shows the correlation between the gap correlation parameter and the gap thickness. The simulation indicates better correlation for thinner gaps. The results from the smallest void show more computational error as expected. Figures 44 and 45 show similar shape, indicating similarity and validity of these approaches within limitations. The slopes of the width ratio and the correlation parameter are high for thin gaps and the slopes decrease to near zero for gaps larger than 0.10 in.

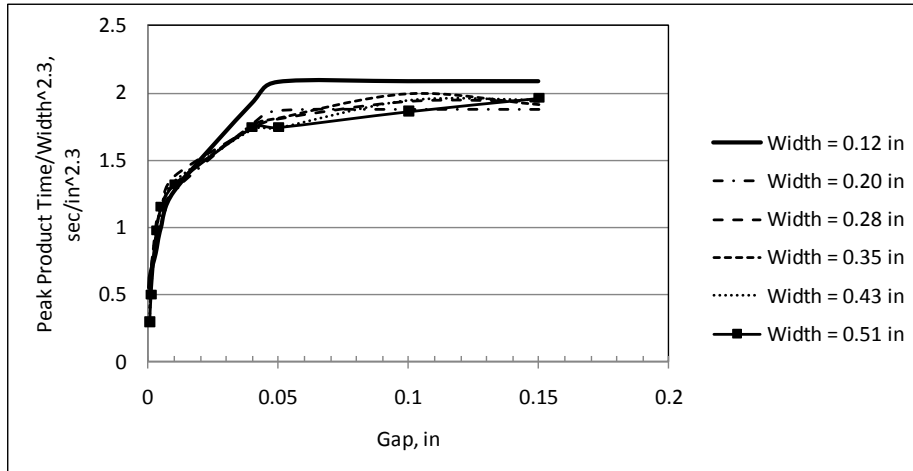


Figure 45: Peak Product Time/Width^{2.3} versus Gap Thickness on Square Voids Using ThermoCalc Simulation

Similar to the simulated results of Fig. 45, a gap correlation parameter (peak product time/half-max width²) is calculated for the experimental RCC data used in Fig. 44. The results are plotted in Fig. 46. Figure 46 provides evidence of correlation between the gap correlation parameter and the gap thickness. Figure 46 is very similar to Fig. 44. Use of the IR Contrast simulation is necessary in computing Fig. 44,. However, only measurements on the contrast evolution are needed in computing Fig. 46. Although, Figs. 45 and 46 are similar, the input data and the gap correlation parameters used by the two are different and can not be compared quantitatively. It should be noted that the data used in Figs. 44 and 46 comes from the same RCC specimens that are similar to that shown in Fig. 69. Considering the unaccounted variability in the data from specimens, Figs. 44 and 46 demonstrate a reasonable correlation of the width ratio and the gap correlation parameter with the gap thickness.

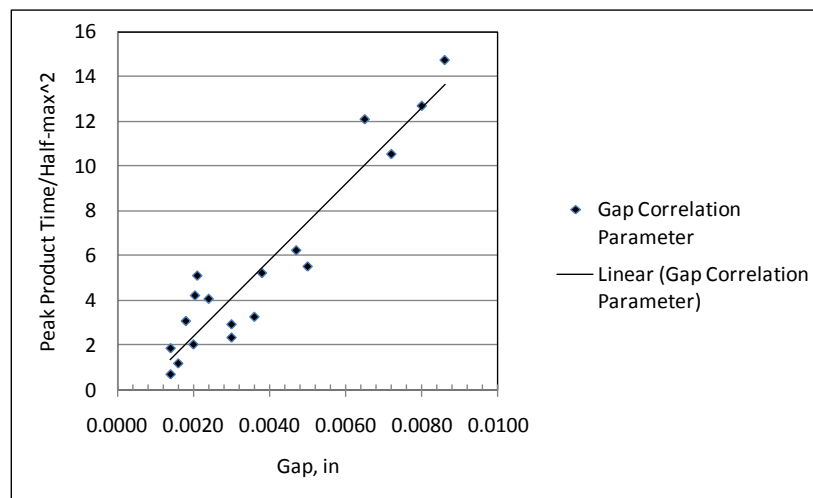


Figure 46: Experimental Data of Peak Product Time/Half-max Width² versus Measured Gap Thickness on Linear Voids in RCC

21. Conclusions

The IR Contrast approach provides two methodologies to analyze the flash thermography video data for characterization of delamination-like anomalies. The first methodology involves measurements such as the peak contrast, peak product time, peak time to contrast ratio, persistence energy time and peak time which can be plotted against the location of the measurement. These measurements show some correlation to the anomaly depth (peak time to contrast ratio), width (half-max) and gap (ratio of peak product time to half-max width). These measurements are also applicable to measurement of surface cracks.

The second methodology involves matching the calibration-based predicted contrast evolution to the measured contrast evolution. The matching of the simulated evolution to the measured contrast evolution provides size and depth of the equivalent flat-bottom hole or equivalent uniform gap with known attenuation. The EFBH (or EUG) depth and diameter are shown to bear correlation to the width, depth and gap thickness of the measured anomaly. Comparison of the EFBH (or EUG) evolutions with measured contrast evolutions, to provide evaluation of delaminations in terms of depth (EFBH or EUG depth), width (half-max), gap thickness (width ratio of EFBH diameter to half-max width) and presence of surface cracks (EFBH diameter and depth estimations), confirms this hypothesis.

The half-max edge detection is considered to be the primary measurement of the width and the IR Contrast EFBH/EUG diameter prediction is considered to be the secondary. Any difference in the two width measurements is thought to be due to non-uniformity of the gap thickness, value of gap thickness, and heat transmissivity across the delamination as well as the limitations of the two estimations. Both the half-max and the EFBH provide analysis of the area of delamination within certain fractional range of attenuation that is weighed heavily by the width containing a relatively thicker gap in the center (primary region of measurement) and very little by the thin gap portion of the delamination at the periphery. The width ratio provides correlation with the delamination gap thickness. The paper provides information on the IR Contrast/half-max analysis software applications.

22. Recommendation for Analyzing Linear Delaminations

The analysis addresses the tapering nature of the delamination gap or the bridging between delaminations to some extent. The boundary of delamination needs to be located non-destructively although it can be determined using destructive microscopy for establishing experimental correlation. For a nonmetal like RCC, the heat flows through the air gap if the gap thickness is less than about 0.010 inch. The contrast evolution is attenuated to 50 percent at about 0.0005 inch to 0.001 inch of air gap thickness. In practice, a gap of approximately 0.001 inch has been observed on many in-family specimens with delaminations. Also, the peak time profile indicates that the contrast map

is likely to be close to the contrast map for 50 percent attenuation for these specimens. Therefore, it is recommended to choose an attenuation level of 50 percent for the EUG analysis as the lower bound. Similarly, the 0 percent attenuation is also recommended for the EFBH analysis as the upper bound. For conservatism, a larger of the two width estimates is recommended especially when half-max boundary cannot be established due to low signal to noise ratio. The length (length-to-width aspect ratio) effect correction is recommended for the EUG estimations. Also, depending upon the delamination depth and width, the EFBH estimations are recommended. Analysis of the validation data should help in choosing the right attenuation level. It is postulated that, although delamination gaps less than 0.0005 inch do exist, they are likely to have smaller continuous areas (short in length and width). These gaps are likely to be separated by material continuity or contact. In order to apply higher attenuation level such as 70 percent, the assumption that the IR evolution is extracted from a continuous gap is necessary. Also smaller gap delaminations may not be detectable by the IR technique due to low signal to noise ratio.

Comparison of the adjusted 50 percent attenuation width (or EFBH diameter) with the half-max width allows assessment of the effective gap thickness in the span bounded by the half-max width. If we call the 50 percent attenuation gap as the standard gap, then we can describe the gap thickness as thicker than, thinner than, or equal to the standard gap. If the half-max width is larger than the adjusted 50 percent attenuation width ($\psi_{\mu 50\%} < 1$), then the delamination gap is thinner than the standard gap. If the half-max width is smaller than the adjusted 50 percent attenuation width ($\psi_{\mu 50\%} > 1$), then the gap is thicker than the standard gap. If the half-max width is equal to the adjusted 50 percent attenuation width ($\psi_{\mu 50\%} = 1$), then the gap thickness is equal to the standard gap thickness. Here the real gaps may not be uniform, and the gap thickness assessment is meant to relate only to the average gap thickness. Experimental data shows positive correlation between the width ratio (e.g. $\psi_{\mu 0\%}$, $\psi_{\mu 50\%}$ etc.) and the actual gap thickness. Conversely, the correlation between the width ratio or the gap correlation parameter and the delamination gap can be established and then used in the evaluation of the delamination gap by measuring the width ratio.

Although it may not be necessary, the equivalent diameter estimates can be further refined by using the estimated gap thicknesses. Thus, once the gap thickness versus the measurement ROI location plot is established, it can be converted to the attenuation versus the measurement ROI location. See Fig. 21. Having known the attenuation, an appropriate calibration curve can be chosen to perform the EUG analysis providing the EUG diameter and depth. The corrected EUG diameter would provide an estimate of the localized width and the EUG depth would provide the depth of the delamination. Thus, the depth, width and the gap thickness can be assessed within limitations.

The half-max width estimation is also affected by the non-uniformity of the gap thickness to a lesser extent than the EFBH diameter estimation. The half-max width estimation is also affected by the pixel size in comparison to width of the feature being measured. This error can be reduced by interpolating between pixels. A larger of the half-max and EFBH

(or EUG) width estimate is recommended if a gap thickness value or attenuation level is assumed. Based on the validation data, a lower percent threshold (e.g. 40 percent) may be better suited for more conservative half-max width estimation. The half-max boundary location is estimated locally while the EFBH (or EUG) boundaries are estimated symmetrical about the measurement ROI's. For monitoring the indication growth, both the half-max boundary and the EFBH diameter can be used. The half-max and the EFBH (or EUG) width estimations have limitations in evaluating the real delamination data. Therefore, it is recommended to use both estimations and the width ratio as both estimations allow conservative compensation for the effect of gap non-uniformity and gap thickness variation.

REFERENCES

1. Maldague, X. P. V., *Nondestructive Evaluation of Materials by Infrared Thermography*, Springer-Verlag London, (1993).
2. Carslaw H. S. and Jaeger J. C., *Conduction of Heat in Solids*, Clarendon Press, Oxford, (1959).
3. Spicer J. W. M., *Active Thermography for manufacturing and Process Control*, Short Course Notes SC05, Thermosense, SPIE – The International Society for Optical Engineering, Orlando, FL, (April 1995).
4. Software: EchoTherm and Mosaic, Thermal Wave Imaging, Inc. Ferndale, MI, 48220, 2008.
5. Software: ThermoFit Pro, Introscopy Institute, Tomsk, Russia, 2005
6. Software: ThermoCalc-3D, Introscopy Institute, Tomsk, Russia, 2005
7. Koshti A. M., *Estimating Temperature Rise in Pulsed Thermography using Irreversible Temperature Indicators*, Proc. SPIE vol. 4702, p. 191-201, Smart Nondestructive Evaluation for Health Monitoring of Structural and Biological Systems, San Diego, CA, March 2002

ACKNOWLEDGEMENTS

The IR Contrast sub-team primarily constituted Dr. Ajay Koshti (ES4, NASA JSC), Walter Wilson (ESCG) and Prof. Chelakara Subramanian (Florida Institute of Technology). Dr. Ajay Koshti was the principal investigator and software developer for the IR Contrast analysis portion of the software. Walter Wilson developed a portion of the software that included the half-max boundary and IR Contrast data extraction. Dr. Chelakara Subramanian (under contract with Engineering Support Contract Group ESCG) reviewed several reports and provided technical evaluation and valuable input towards technical writing and editing. The teamwork was coordinated on a weekly basis. ESCG support was coordinated by John Knesek (ESCG) and Julie Henkener (NASA JSC).

This work was supported by several individuals from the Orbiter Project Office including Dr. Justin Kerr, Richard Russell and Frank Lin. The project was assessed periodically by Justin Kerr. Justin Kerr and Frank Lin were instrumental in providing the primary funding to undertake this project.

Many other individuals contributed, notably Dr. William Winfree (NDE Branch Chief, NASA LaRC), Dr. William Prosser (NESC Technical Fellow for NDE, NASA LaRC), Patricia Howell (NDE, NASA LaRC), Dr. Thomas Elly (NDE, NASA LaRC) through their technical comments. Eric Burke (NDE, USA) and the NDE sub-team led by him contributed through discussions during team meetings, peer review meetings and the work accomplished by the NDE sub-team complemented the IR Contrast work. Microscopy work by Beth Opila (NASA GRC) was used in the case study of the IR Contrast. James Landy (NDE, USA) and Jeffery Elston (NDE, USA) provided some of the flash thermography data used in this work.

Alvaro Rodriguez (Thermal Design Branch, NASA JSC) and Ronald Lewis (Thermal Design Branch, NASA JSC) reviewed the results, participated in the IR Contrast training and provided direction for the validation analysis. Steven Rickman (NASA Technical Fellow for Passive Thermal, NASA JSC) reviewed the theoretical aspect of the IR Contrast technique and this report. He provided valuable comments that have been incorporated in this report.

NASA management notably Brad Files, Edgar Castro, Stephen Altemus, Steve Poulos and Bud Castner provided approval to undertake this project. The engineering directorate provided some funding under the IR&D during 2009.

ESCG NDE team members Ovidio Oliveras (ESCG), Norman Ruffino (ESCG) and Eddie Pompa (ESCG) and intern Natalie Spencer provided support by learning the IR Contrast applications to analyze flash thermography data and providing valuable feedback. The PI thanks his family for support to work on this project.

APPENDIX: Calibration Steps in the IR Contrast Application

Calibration standards with FBH's are needed for the calibration. Choose two depth values (lower limit and higher limit) to establish a depth range of interest. At each depth, choose low and high values (lower limit and higher limit) for diameter to establish a diameter range of interest. Choose several diameter sizes that span the range of diameters. Fabricate the standards and measure the depth and diameter accurately. Assign a unique number to each hole. It is important to know the thermal diffusivity of the material accurately. If the diffusivity is not known, measure the diffusivity using a through transmission flash thermography technique. If the part emissivity is lower than 0.75, then apply a high emissivity coating. In order to use the calibration based analysis, parts with the same material will have to be inspected with the same emissivity coating.

Next, perform the flash thermography inspection and capture contrast evolutions on the holes of the chosen standards. Open the IR Contrast application. Choose the material that has the closest diffusivity to the calibration standard. Choose the frame rate for the simulation that matches the frame rate in the actual contrast evolutions. Choose the depth constant so that the diffusivity input times the depth constant matches the estimated diffusivity of the material. If the chosen diffusivity value is in error, it will cause changes in the calibration curves. As long as the same diffusivity value is chosen during the data analysis, it will not cause any additional errors. Thus, the calibration curves are referenced to the ratio of the part diffusivity and assumed diffusivity (diffusivity input times the depth constant). The assumed diffusivity can be changed by changing value of the depth constant.

Open a contrast evolution from one of the lower depth holes using the IR Contrast application. Always examine for levelness of the contrast evolution. The contrast for the beginning frame (first frame) and the end frame shall be at same level and close to zero. If the evolution is not level, re-extract the contrast evolution by choosing a different reference ROI. Input the correct diameter and depth of the FBH. Refresh the plot. Ensure that the "un-calibrated" mode is on. Ensure that other inputs (e.g. frame rate, depth constant etc.) are correct. The simulation may not match the actual contrast evolution. Note the peak time (or frame) of the actual contrast evolution. Change the diameter constant such that the peak time of the simulation matches with the actual peak time. Change the amplitude constant to match the amplitude of the signal. Note the flaw size parameter (A_c), diameter constant and the depth constant values. Load another contrast evolution from a hole with the same depth but a different diameter. Repeat the process. Analyze all holes at the low depth. Repeat analysis of contrast evolutions of all holes at higher depth. Plot the diameter constant and amplitude constant against flaw size parameter. Establish a single best fit diameter calibration curve for both depths.

The amplitude constant data for each depth is likely to indicate a separate trend line. Choose only the low depth flaw amplitude constant versus the flaw size parameter data to establish the amplitude constant calibration curve. Create the calibration file. Calibration file is a text file with a table containing three columns. The first column is the flaw size

parameter. The second column is the diameter constant and the third column is the amplitude constant. The lowest flaw size parameter value is 0.01 and the highest is 1.0. Choose at least 10 values of flaw size parameter in the table.

Open the IR Contrast application if not open. Choose “calibrated” mode and load the calibration file. Load a contrast evolution from a low depth hole. Verify other input values. Use “Auto-fit” window to find automatic match of the simulation with the signal. Observe if the input values of diameter and depth in the simulation match with the same for the actual hole. If the match is good for all holes at low depth, load a contrast evolution of a hole with high depth with highest gamma. Unclick the “Auto-fit” option.

Open the amplitude factor calibration window. Choose “apply amplitude factor” calibration. Type the low depth value as the base depth value. Type the actual depth and diameter values in the simulation input. Observe the simulation contrast evolution. Use the amplitude factor slope of 1 for the base depth. Change the amplitude factor slope and refresh the plot to match the simulation with the actual signal. Note the amplitude factor slope value. Repeat the process by loading another high depth contrast evolution. Note the amplitude factor slope that provides the best match. The amplitude factor slope may be positive or negative. Average all the slope factors and use the average value. Re-analyze all the high depth contrast evolutions using the same amplitude factor value.